CHALMERS

Laser cutting in Ti-6Al-4V sheet: DOE and evaluation of process parameters Informative

Diploma work in the Master programme Materials Engineering

NILS ANDERSSON
CARL GRANBERG

Diploma work No. 164/2015
Department of Materials and Manufacturing Technology
CHALMERS UNIVERSITY OF TECHNOLOGY
Gothenburg, Sweden

Laser cutting in Ti-6Al-4V sheet: DOE and evaluation of process parameters Informative

by

NILS ANDERSSON
CARL GRANBERG

Diploma work No. 164/2015
at Department of Materials and Manufacturing Technology
CHALMERS UNIVERSITY OF TECHNOLOGY
Gothenburg, Sweden

Diploma work in the Master programme Materials Engineering

Performed at: Material and Manufacturing Department
GKN Aerospace
SE - 46 181 Trollhättan

Supervisor(s): Prof. Uta Klement
Materials and Manufacturing Technology
Chalmers University of Technology
SE - 412 96 Gothenburg

Examiner: Prof. Uta Klement
Department of Materials and Manufacturing Technology
Chalmers University of Technology,
SE - 412 96 Gothenburg

Laser cutting in Ti-6Al-4V sheet: DOE and evaluation of process parameters Informative
NILS ANDERSSON, CARL GRANBERG

Diploma work no 164/2015
Department of Materials and Manufacturing Technology
Chalmers University of Technology
SE-412 96 Gothenburg
Sweden
Telephone + 46 (0)31-772 1000

[Reproservice]
Gothenburg, Sweden 2015

Laser cutting in Ti-6Al-4V sheet: DOE and evaluation of process parameters Informative

NILS ANDERSSON, CARL GRANBERG

Department of Materials and Manufacturing Technology
Chalmers University of Technology

SUMMARY

Different Titanium alloys are frequently used in the Aerospace industry owing to its attractive properties at high temperature service. Manufacturing of those parts are performed by different conventional and non-conventional methods where Laser Cutting are one of the latter. High demands on quality and security within the aerospace industry results in high requirements on the part after cutting. To accommodate the requirements it is necessary to possess knowledge about how the laser cutting process affects the material in terms surface finish and heat affected zone. Therefore, this thesis aims to investigate the effect of different laser cutting process parameters, namely material thickness, cutting speed, beam power, gas pressure and lens focal point and how a variation of their level affect the properties of a cut part.

The alloy used for this study is Ti-6Al-4V, an alloy frequently used for manufacturing of engine parts in the aerospace industry. Experiments were planned via the statistical method Design of Experiment and two separate full factorial test plans were prepared.

Samples were cut from different sheet thicknesses of the alloy Ti-6Al-4V according to the test plan. Sections from the samples were later on evaluated by measuring the heat affected zone, the surface irregularity and burr height. Additional hardness measurements not included in the test plan was also performed.

The results showed that the material thickness and cutting speed were the parameters with strongest impact on the result. Also beam power and gas pressure showed an impact. Increased hardness in the heat affected zone was observed. Some measurements contained to much noise which led to that they could only serve as indicative and no conclusions could therefore be drawn from them.

Keywords: Laser cutting, Ti-6Al-4V, aerospace application, material thickness, cutting speed, beam power, gas pressure and lens focal point, Design of Experiment.

Note from authors.

This project is carried out at the Material and Manufacturing Department of GKN Aerospace in Trollhättan.
We would like to thank our supervisors Joakim Idetjärn and Uta Klement for all the help and advices throughout this thesis work. We would also like to thank Fredrik Niklasson, Jimmy Johansson and Pär Ingemansson for extra guidance, Trestads laser for the help of conducting our experiments as well as Jörgen Magnusson at Innovatum for the help with the Burr classification.

Nils and Carl, Gothenburg, June 2015

Table of content

1 Introduction

1.1 Background

This project is carried out at the Material and Manufacturing Department of GKN Aerospace in Trollhättan. They are responsible for all the conventional and non-conventional machining operations at GKN. Laser cutting is one of the non-conventional methods used by GKN in the aerospace industry. At the moment GKN is using laser cutting as a method of machining. When GKN gain more knowledge and data on how laser cutting parameters affect the cut material, more optimized requirements could be used.

1.2 Purpose

The purpose of this thesis work is to assess how different laser cutting parameters used with both Argon and Nitrogen as assistant gas affects Ti-6Al-4V sheets, to reveal which process parameters of Laser cutting that has the greatest effect on the cut part. The thesis work will be of help for GKN when setting requirements on a laser cut parts.

1.3 Problem definition

This thesis work is defined from the following questions:

- How do the process variables of laser cutting affect the cut surface and surrounding material?
- What are the limiting aspects of laser cutting that can be important when putting requirements on laser cut parts?

1.4 Scope

This thesis includes

- A comprehensive background study of the material and process used.
- Process parameters selection.
- Construction of test-plans.
- Laser cutting of samples from the test-plan.
- Sample preparation of all samples including mounting, grinding, polishing and etching.
- Evaluation of the cut samples by:
  - Measurements in the optical microscope.
  - Hardness measurements of selected samples.
  - Classification and measuring of burrs.

- Analyze of the result from evaluation of the samples in Modde 10.0.
- A discussion regarding the results
- Conclusions from the analysis

2 Theory

In this chapter information is presented about laser cutting in general as well as results from studies that have been done in same field as this thesis work.

2.1 Titanium alloys

Ti-6Al-4V is the most used Titanium alloy today where the aerospace industry accounts for over 80% of its usage (Boyer, Welsch and Colling, 1994). The reason for the frequent use of this alloy in the aerospace field is its high strength to weight ratio, high fracture toughness, high strength and stiffness at elevated temperatures, excellent corrosion resistance, fatigue resistance and ability to withstand creep at fairly high temperatures. Components made from Ti-6Al-4V can be wrought, cast or made from powder metallurgy, with wrought alloys being the most common in the aircraft industry (Pandey & Dubey, 2012). Virtually all types of conventional machining operations such as turning, milling, drilling, grinding, etc. are employed in the production process of aerospace components. However, the machinability of Titanium and its alloys are considered to be poor. High temperatures at the tool/workpiece interface owing to the low thermal conductivity significantly affect lifetime of the tool as well as the properties of the material. Moreover, the high temperature strength together with a low Young's modulus further impairs the machinability (Ezugwu & Wang, 1997).

2.2 Crystal structure

Titanium alloys are stable at different temperatures either with a hcp or a bcc crystal structure. Pure Titanium consists of hcp crystal structure at room temperature and is referred to as alpha Titanium. At a temperature of 882 °C, there is an allotropic transformation from hcp alpha Titanium to bcc beta Titanium, the beta phase extends up to the melting temperature of 1672 °C. The hcp/bcc transformation temperature is not constant and can be altered by alloying elements that shift the transus line either up or down. Aluminum, Nitrogen and Oxygen are elements that move the transition line towards higher temperature and hence are stabilizing alpha-phase. Vanadium has the opposite effect on the transition line and is thus a beta-stabilizer (Leyens & Peters, 2003). A two phase alpha + beta field is developed by the addition of alpha and/or beta stabilizing elements. This two phase field is stable at room temperature depending on the relative proportions of each of the stabilizing elements. The beta-stabilizing elements can be further divided into isomorphous or eutectoid elements depending on their impact on the appearance of the phase diagram. Vanadium and molybdenum are examples of elements that are miscible in the beta phase, i.e. they have a high solubility and are called isomorphous elements. Manganese, Iron and Chromium are examples of elements that form eutectoid systems with Titanium at a eutectoid temperature of 333 °C below the transition temperature of unalloyed Titanium. Hence, when Ti-6Al-4V is alloyed with 6 % percent of Aluminium and 4 % of Vanadium the microstructure at room temperature will be of alpha+beta structure (Voort & George, 2004).

2.3 Cooling

Cooling Ti-6Al-4V from liquid state will result in a transformation from liquid to a bcc-beta structure.
Two different transformations are of interest when cooling from the beta field. First, precipitation of alpha upon cooling from beta to alpha + beta occurs by transformation of the closed packed {110} plane in the beta phase to the close packed {0001} basal plane in the hcp alpha phase. Since the distance between the close packed {110} planes in beta is slightly smaller than the distance between the {0001} basal planes in alpha, there is an atomic distortion and a small contraction of the alpha c-axis upon beta to alpha transformation. This leads to a reduction of the c/a ratio below the critical value for an ideal hexagonally close packed atomic structure (D.A. Porter, 2009). Since the bcc beta unit cell has 6 slip systems and 2 slip directions, there is a maximum of 12 possible orientation relationships to hcp alpha. Thus, nucleation and growth of alpha-phase within the prior beta-phase follows any of those directions. Growth takes place in a lamellar Widmanstätten manner with beta phase as thin layers between the alpha plates (Leyens & Peters, 2003).

2.4 Laser cutting

Lasers can be categorized through the active medium used. Solids, gases, semiconductors, chemical lasers and metal vapor lasers are some examples of the active medium used in a laser. All these different lasers have their specific wavelength and application. Laser cutting is mostly performed with CO_2 lasers or fiber lasers (Weber, 1999).

2.4.1 CO_2 laser

A CO_2 laser is as its name implies using CO_2 as active lasing medium. The cavity containing the active medium is filled with Carbon dioxide as well as Nitrogen and Helium. The proportions of the mixture are often typically around 1:8:20 by volume, respectively of the gas mixture elements/molecules. Nitrogen and Helium are both added to increase the efficiency of the CO_2 laser.

Most CO_2 lasers work according to the same principle which hereinafter will be explained: The gas mixture of CO_2, Nitrogen and Helium is bombarded by electrons which at high speed collide with the Nitrogen molecules which thereby receive an excited state. This higher energy state of Nitrogen is close to the upper lasing energy of CO_2. When the Nitrogen molecules collide with the CO_2 molecules they pass on this energy which is thereby exciting the CO_2 molecules. A few of these CO_2 molecules are spontaneously relaxing and releasing a photon, when this photon hits another excited CO_2 molecule, it will release a photon as well. These photons will continue to hit other excited CO_2 molecules and thereby creating an exponential development of photons. The helium atoms will later on collide with the deexited CO_2 molecules to take them back to their initial level of energy. This will lead to a temperature increase of the Helium molecules (Powell, 1998). For lasing to occur, a population inversion state of the CO_2 molecules is required; the number of excited molecules must be higher than the number of molecules in a lower energy state. When

this state is reached, the light is able to amplify itself. This state is a must for enabling stimulated emission (Steen & Mazumder, 2010).

A cooling system is needed for taking care of the excessive heat from the laser. There are two basic systems of cooling methods which are called "slow flow" and "fast flow". Slow flow lasers are cooled via conduction of the cavity with water or oil as the cooling medium surrounding the cavity. This method is mostly used for low power lasers. Fast flow lasers are kept cool through a system with a heat exchanger and a blower (fan) which circulates the cavity gas mixture. The fast flow cooling system is used for most high power lasers (Powell, 1998).

2.4.2 Fiber laser

A fiber laser is a so called solid state laser in which the active medium is a glass fiber doped with rare earth elements such as Neodymium, Ytterbium and Erbium. Fiber laser can be an interesting alternative to the CO_2 laser, especially when cutting thinner sheets (below 4 mm) or when cutting highly reflective materials. Subsequent welding of edges produced by fiber laser cutting without further machining operations have proven to be of equally mechanical performance as for laser welded milled edges (Scintilla, Palumbo, Sorgente and Tricarico, 2013)

2.5 The cutting process

The cutting of a material can be carried out in several ways, such as vaporization cutting, melt and blow cutting and reactive fusion cutting. The melt and blow method is using the laser beam to melt the workpiece and a pressurized gas to blow away the molten material. Since it is using only half the energy needed for "vaporization cutting" and the HAZ is kept in a range of tenth of micrometers, the melt and blow process is the major cutting method used for metals such as Titanium (Steen & Mazumder, 2010). In this method of cutting, the leading end of the beam is melting the material and heat conduction is responsible for melting the material in front of the beam which guides the beam into a straight cut. At low speeds, only the front of the beam is interacting with the material while the rest is passing through the kerf. A part of the laser beam will be absorbed and some will be reflected at the surface of the material.

At the lower region of the kerf, a thickening of melt can be a problem. This can be caused by a gathering of melt coming from the top of the cut, it can also be related to surface tension and oxide films, a combination of these together with a low pressure region created by the gas flow can result in melt being sucked backwards and subsequently solidifying as dross (Steen & Mazumder, 2010).

During the laser cutting process, most of the heat melts and/or vaporizes the material which is then blown away by the assist gas.
The rest of the heat is conducted into the material, changing the microstructure of the material, resulting in the heat affected zone (HAZ). The outermost region of the HAZ, adjacent to the re-melted and solidified material (recast layer) can be heated to just below the melting temperature. As the heat source is moving away, the cut edge surface is rapidly cooled due to heat conduction into the matrix and convection of the

assistant gas flow. Martensitic transformation can occur if cooling rate is sufficiently high. Though, in Titanium this does not have a strong impact on hardness which increases by approximately 10 %. (Leyens & Peters, 2003) (Shanjin &Yang, 2006). The thickness of the HAZ and recast layer is strongly dependent on laser cutting parameters such as pulse frequency, type and pressure of assist gas, beam intensity and cutting speed (Scintilla et al. 2013).

Laser cut surfaces can be divided into three zones, a top zone, an intermediate zone and a bottom zone depending on the surface morphology resulting from the cutting process. The top zone where the laser beam first interacts with the material is relatively flat and has a small width of a few microns. Typically for the intermediate zone are the so-called primary striations. They are periodic and have the same frequency as the laser pulses. As the beam penetrates deeper in the material there is a decreasing effect of the laser pulses and the gas flow becomes the dominant factor. The bottom zone is characterized by irregular undulations (Shanjin & Yang, 2006).

2.6 Burr

Burr is an unwanted piece of material on the edge of a workpiece caused by the manufacturing process. There is no universal standard that defines burr and many companies have their own way of classifying it, although the root thickness and the burr height are two geometrical parameters often used to describe the nature of a burr. Burrs are often sharp and can act as fatigue initiation place due to stress concentrations. Burr may become detached from parts during operation which can cause loss of function. The sharpness can also cause injuries during assembly. Therefore, deburring operations which are both costly and time consuming are necessary (Aurich et al. 2009).

2.7 The influence of laser cutting parameters on the cut edge

2.7.1 Different assist gases

Titanium is highly reactive at elevated temperatures. Usage of Oxygen as assistant gas in Titanium cutting will lead to an exothermic oxidation reaction. This reaction will create an uncontrolled melt front resulting in a workpiece with a large kerf, bad surface roughness and a wide HAZ with presence of microcracks (Pandey & Dubey, 2012) and (Shanjin & Yang, 2006). Nitrogen is in many cases acting as an inert gas when cutting in e.g. stainless steels (Anon, 2015), but in Titanium alloys it will react and create Titanium Nitrides. They are hard particles which severely harden the material, in commercial pure Titanium up to 2 times and in Ti-6Al-4V up to 3 times (Almeida et al. 2006). The TiN will appear as a yellowish surface in the cut edge (Tirumala Raoa, Kaul, Tiwara, and Nath, 2005). Using air as assistant gas will lead to absorption and reactions of both Oxygen and Nitrogen in the cut edge which causes both an uncontrolled melt front and formation of hard and brittle oxides and nitrides. This will result in a material with both reduced fatigue life due to the embrittlement of TiN and a large kerf, bad surface roughness and a wide HAZ as a consequence of the Oxygen (Ezugwu & Wang, 1997). When Titanium is exposed to air at temperatures above 600°C, diffusion of Oxygen into the surface layer starts taking place. Oxygen is

stabilizing alpha phase and the resulting surface layer is known as alpha-case, which is a hard and brittle zone with reduced mechanical properties like ductility and fatigue resistance. The alpha-case layer varies in depth depending on time and temperature during which the material is subjected to Oxygen. When cutting with an inert gas like e.g. Argon, formation of the alpha-case layer can be avoided (Gurappa, 2003).

Surface roughness can be highly affected by the usage of different assist gases. Studies made on cutting in Aluminum showed that the use of Nitrogen as assist gas resulted in formation of nitrides. The process in the cut edge when forming the nitrides leads to increased surface roughness (Davim, 2013).

2.7.2 Gas pressure

The assistant gas is besides its main purposes also cooling the melt. The cooling effect is dependent on factors such as the thermal conduction of the gas and gas pressure (Tirumala Raoa et al. 2005). A high gas pressure is leading to a smaller HAZ since a high gas pressure provides more convection of heat (Shanjin & Yang, 2006).
To avoid dross formation when cutting with an inert gas the gas pressure should be as high as possible (Steen & Mazumder, 2010).

2.7.3 Cutting speed

Tirumala Raoa et al. observed light yellow and blue films on the cut edge. This color change was more distinct at higher cutting speeds since higher cutting speeds lead to more hot dross formation because it reduces the time for the gas to blow away the molten metal and thus an extended exposure time to Oxygen and Nitrogen present in the atmosphere (Tirumala Raoa et al. 2005). Higher gas pressure limited the color change to the bottom of the kerf while lower extended it towards the top.
The energy density of the laser beam is in inverse proportion to the cutting speed, thus a high cutting speed results in that less amount of heat energy is conducted into the workpiece. HAZ stands in proportion to heat energy input. Thus, high cutting speed results in a small HAZ (Shanjin & Yang, 2006), (Teixidor, Ciurana and Rodriguez, 2014).

2.7.4 Beam power

Beam intensity is a combination of beam power and irradiated area. A high intensity makes it possible for faster cuts since it causes the material to heat up quicker. Thus, less time is given for heat to conduct into the material. It is the beam intensity that determines the thickness of the material being able to be cut (Karatas, Keles, Uslan and Usta 2006). A higher beam power in combination with high cutting speed results in increased dross formation. High beam power leads to more molten metal, hence more dross will be present in the cut edge (Teixidor et al. 2014).

2.7.5 Focal position

Focal length is defined as the distance from the center of the lens to the point of focus. The laser beam is said to be focused within a range called the depth of focus, in which the intensity of the laser beam is sufficiently high. A short focal length results in high beam intensity but a small depth of focus, and thus is more suitable for cutting of thinner materials. A longer focal length gives a larger depth of focus but also decreases beam intensity. Thicker materials are more suitable to be cut with a large focal length. Optimum focus position is critical in the cutting process and has a major influence on the quality of the cut edge in terms of surface roughness and amount of dross at the bottom of the cut surface (Thombansen, Hermanns and Stoyanov 2014). A 65 mm lens is suitable for cutting sheets up to 6 mm in thickness (Semiatin, 2010).

3 Method

This section of the report will account for the methods used and the experiments carried out in order to collect data and evaluate the laser cutting process of a Titanium sheet.

3.1 Experimental parameter

The process parameters that were chosen to be evaluated were chosen based on experience from Trestads Laser AB and GKN together with research made on similar studies of laser cutting in Titanium.

Earlier investigations made on the influence of gas pressure, beam power, cutting speed and type of gas (Pandey & Dubey, 2012), (Almeida et al. 2006), (Shanjin & Yang, 2006), (Tirumala Raoa et al. 2005) confirms the interest of those process parameters. Trestads Laser changes focal position based on wear of the lens where they have by experience noted that a worn lens works better with a focus deeper into the workpiece and vice versa with an unworn lens. Other studies have shown that focus position have effect on the quality of the cut edge as well as influences the material thickness that is able to be cut (Thombansen et al. 2014). Three sheet thicknesses were selected to be evaluated. The chosen process parameters to vary and their levels can be seen in table 1. The fixed process parameters can be seen in table 2.

Table 1. Selected process parameters for both the Argon and Nitrogen series.

Parameters	**Low**	**Center**	**High**
Material thickness (mm)	1	3,2	6,35
Lens focal length (%)	30	55	80
Beam power (kW)	2	3	4
Cutting speed (m/min)	0,5	1,5	2,5
Gas pressure	12	16	20

The data in the table below have been excluded due to secrecy of GKN Aerospace property.

Table 2. Fixed process parameters for the Argon and Nitrogen series

Parameters	
Lens length (cm)	-
Pulse frequency (Hz)	-
Nozzle stand of distance (mm) Argon/Nitrogen	-
Nozzle orifice (mm)	-

3.2 Design of experiment

The experimental set-up of the samples were prepared with Modde 10 which is a software developed by Umetrics.

Design of experiments is a way to work where statistical methods are used to detect linear effects of factors used and also interaction of factors.
The benefit of using this method compared to using a classic factor by factor experiment set up where one factor is varied while the others are constant are the possibility of both detecting concurrence effects and the ability to reduce the amount of tests.

A high and a low value were chosen for each parameter. These values were used as test values in a full factorial test with two levels. Five parameters with two values generated 32 samples per gas. In addition to the 32 samples 5 samples were cut with identical and intermediate parameter settings between the high and the low value. These five samples serve as noise indicators to ensure the reproducibility of the test set-up. Two sets of experiments was set up, one with Argon as assist gas and one with Nitrogen as assist gas resulting in a total amount of 74 samples. The two test plans can be seen in Appendix A.

3.3 Cutting at Trestad Laser

The experiments were carried out at Trestad Laser AB in Trollhättan. The machine used was a TruLaser Cell 1005 4KW CO_2.

Before the actual test-plans were executed test runs were performed to identify possible parameter combinations that could result in an incomplete cut. The thickest material was cut for this purpose with Nitrogen as assisting gas. Based on these tests it was decided to increase the lowest beam power from 2 to 3 kW, decrease the highest cutting speed from 2,5 to 1,0 m/min and change the highest and lowest gas pressure from 20 to 18 bar. The final parameter settings for the Nitrogen series can be seen in table 3.

Table 3. Final process parameter levels for the Nitrogen series.

Parameters	**Low**	**Center**	**High**
Material thickness (mm)	1	3,2	6,35
Lens focal length (%)	30	55	80
Beam power (kW)	3	3,5	4
Cutting speed (m/min)	0,5	0,75	1,0
Gas pressure	14	16	18

The same changes were made for the Argon series with an additional lowering of the gas pressure resulting in a low and a high value of 12 and 14 bar. The parameter levels for the Argon series can be seen in table 4.

Table 4. Final process parameter levels for the Argon series.

Parameters	Low	Center	High
Material thickness (mm)	1	3,2	6,35
Lens focal length (%)	30	55	80
Beam power (kW)	3	3,5	4
Cutting speed (m/min)	0,5	0,75	1,0
Gas pressure	10	12	14

The piercing time was also changed because too much heat was generated. See piercing settings for both Argon and Nitrogen series in table 5.

Table 5. Piercing settings for both the Argon and Nitrogen series.

Parameters	Argon	Nitrogen
Time (s)	5	1
Nozzle stand of distance (mm)	6	6
Blow out time (s)	2	0
Gas pressure (Bar)	0,5	2

3.3.1 Extra samples

For both the Nitrogen and the Argon series additional samples were produced. Ten extra samples were produced outside the regular Argon test-plan for which the cutting speed was increased in a number of steps for all material thicknesses. Six samples were produced outside the regular Nitrogen test-plan in the same manner as for the Argon samples.

3.4 Sample evaluation

The produced samples made from Laser cutting with Argon and Nitrogen were evaluated according to a standard set by GKN which includes HAZ, surface irregularity, and crack measurements. An evaluation of burrs and hardness measurement was also done.

3.4.1 Sample preparation

A drawing of the sample geometry can be seen in figure 1 and a picture showing the selected parts for mounting can be seen in figure 2.

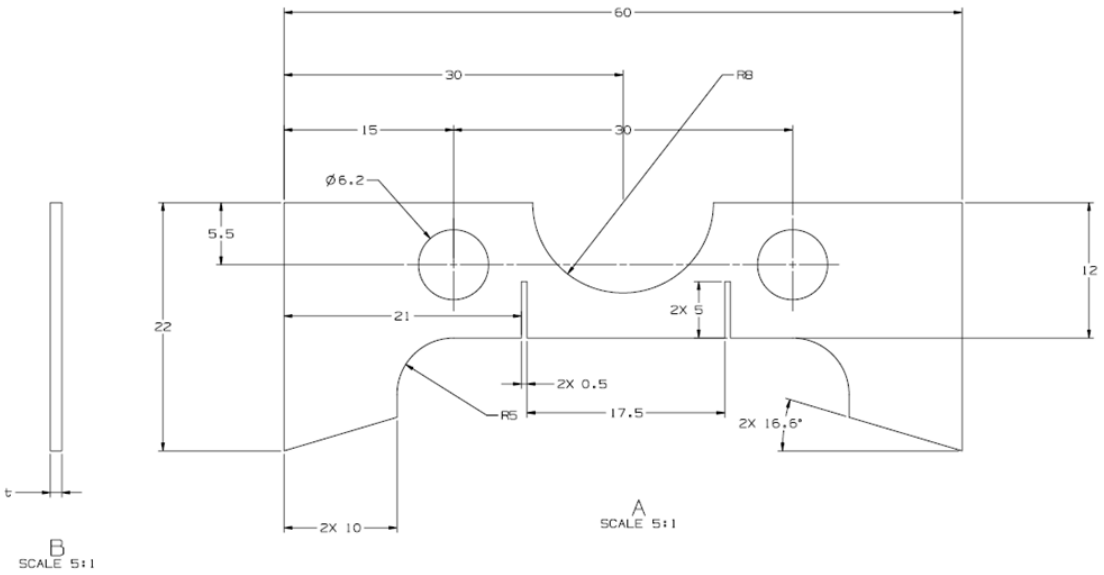

Figure 1. Drawing of the sample geometry.

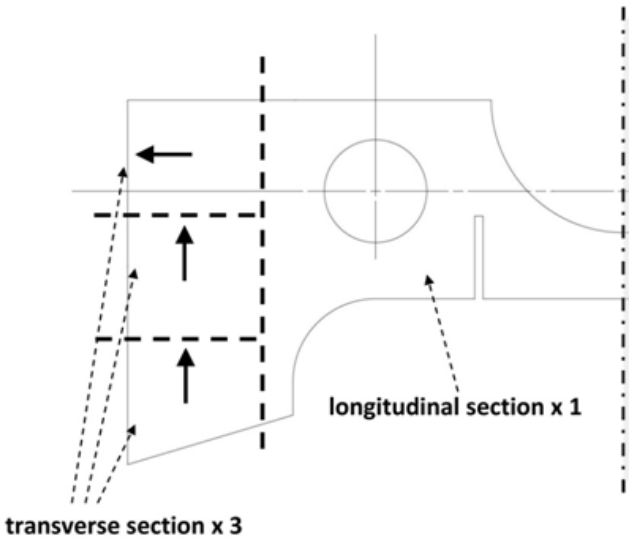

Figure 2. Longitudinal and transverse sections for mounting, arrows indicating which side of the transverse cut that is facing up in the mountings.

Three transverse sections and one longitudinal section from each sample were mounted in Bakelite mounts to enable optical microscopy examination and hardness measurements.
The other half of the samples were kept for burr evaluation and subsequent storage. The samples were at first ground with a course grinding paper to ensure a flat surface. Grinding and polishing were afterwards performed to achieve a mirror like surface (protocol with information about grinding, polishing and etching procedure can be found in Appendix B). The samples were investigated in an optical microscope at a magnification of 100x prior to etching in order to detect possible micro-cracks in the HAZ.

All samples were etched with the ASTM Kroll's for 20-25 seconds. The etching procedure was terminated with rinse water. The samples were afterwards cleaned with alcohol and blow dried with a hot air gun.

3.4.2 HAZ measurements

The HAZ were measured at both the transversal and the longitudinal sections. Optical microscopy revealed two types of structures in the HAZ, an inner brighter structure and an outer darker structure as can be seen in figure 3. Both structures were observed at all locations.
On the longitudinal section, measurements were taken at 20 different locations, and a map with the measured locations can be found in Appendix C. The measurements were taken at a magnification of 100x and 50x at locations with bigger HAZ such as in corners.

The measurements made on the transversal sections were made at 50x magnification at a distance of 0,3 mm and 0,5 mm from the top side of the laser cut edge, respectively. The distances were selected in order to compare with the longitudinal HAZ values and to see how HAZ is varying in the thickness direction.

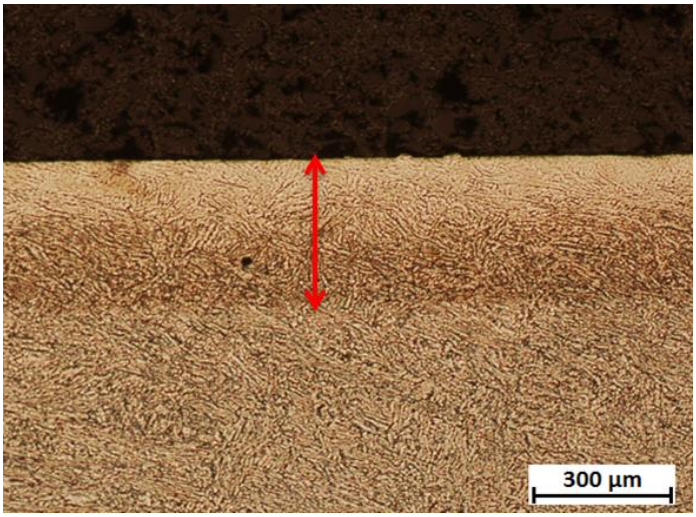

Figure 3. Light optical microscope image of a laser cut edge. The arrow illustrates how the HAZ measurements were performed on the longitudinal section.

3.4.3 Surface irregularity

The surface irregularity was measured on the longitudinal section of the samples. 16 locations around the part were selected and the surface irregularity was measured to nearest 5 µm at a magnification of 200x. The locations of the measurements can be seen in Appendix D. A magnification of 500x was used for the Argon series where the surface irregularities were less than 10 µm, in this magnification the surface irregularity was measured to the nearest 2µm. Figure 4 shows how the measurement was performed, the arrow between the two parallel lines represents the surface irregularity measured.

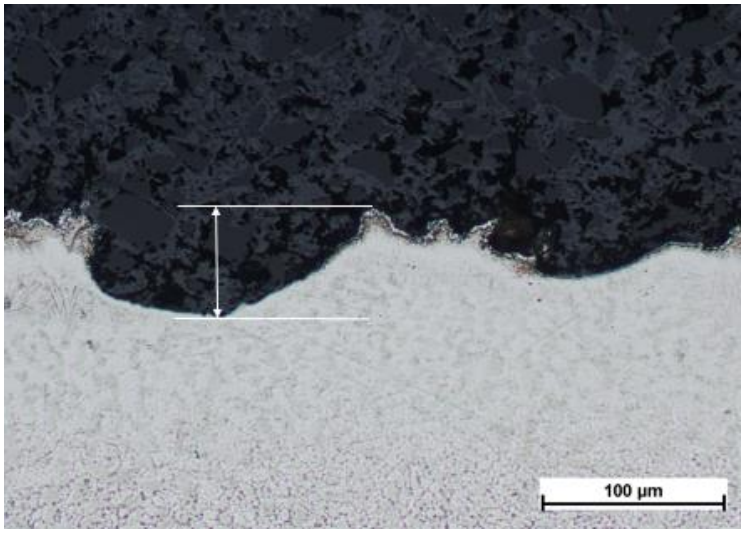

Figure 4. Light optical microscope image illustrating how the surface irregularity measurements were performed.

3.4.4 Burrs

A high degree of burr was observed on all the cut samples. It was therefore of interest to further investigate the burr since it is both costly and time consuming to have it removed by machining.

The burrs were rated on a scale of one to five based on their resistance to be removed. Samples were machined with an abrasive nylon wheel in order to remove the burrs. This is the standard tool used at GKN for deburring in production. Furthermore, the maximum height and average height of the burr were measured.

3.4.5 Hardness measurements

Hardness measurements were performed on selected samples from the argon and nitrogen series, respectively. Samples were selected in such way that material thickness, cutting speed and gas pressure varied between the samples. A Vickers micro-indenter with a load of 50 grams was used. An experiment of producing alpha case was also conducted, the purpose of this experiment was to obtain the hardness of alpha case. A piece of 1mm sheet material was heat-treated in air at 800 °C for 5 hours and was then subjected to hardness measurements.

Figure 5 shows the indentation profile on a longitudinal section. Four indentations at both a distance of 15 µm and 30 µm were made parallel to the surface before proceeding perpendicular to the cut edge with a distance of 15 µm between each indentation. Six indentations were made in the base material. Three of them were made with a load of 300 gram to see a possible deviation compared to with the lower load. On the transverse sections measurements were made on four (on the 1 mm samples) and six (3,2 and 6,35 mm samples) different spots in the thickness direction

as can be seen in figure 5. From these spots, indentations were made in from the surface with a distance of 45 um between them.

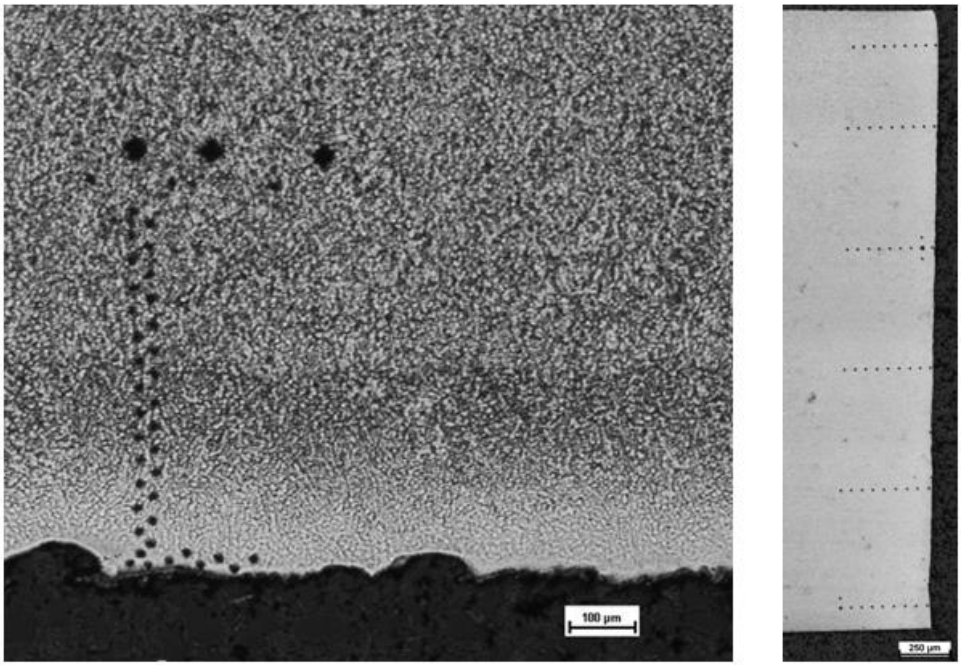

a) b)

Figure 5. Light optical microscope image illustrating how the hardness measurements were made on the longitudinal section in a) and transverse section in b).

Evaluation of data in Modde 10.

The data collected from The HAZ, surface irregularity and burr measurements were ordered in responses for Modde 10. A response from the HAZ from both the longitudinal and transverse sections were created as well as responses of average values from the surface irregularity measurements and the burr measurements.

When analyzing the data in Modde mainly the following four parameters were taken into consideration in an early stage to see which responses to proceed further with:

- R2: The R2 value in Modde describes how well the model fits the data. A large R2 value means that the variation of the response is explained by the model.
- Q2: The Q2 value tells how well the model can predict new data, i.e. how well the model can predict variation.
- Model validity: Gives a measure of the validity of the model. If larger than 0.25 there is no lack of fit and the model error is in the same range as the pure error.

- Reproducibility: This is the variation of the response under the same condition. In this case it is the variation in responses of the mid-level samples that were cut with the same parameter settings. In order for the model to be valid the reproducibility should be as high as possible. A minimum of 0.8 is desirable where 1 means that there is no variation in the responses.

A replicate plot of all responses was conducted as a first step in analyzing the data from the HAZ, surface irregularity and burr measurements. Figure 6 shows an example of a replicate plot of the overall Nitrogen series average HAZ measurements.

The samples named from one to 32 are representing the high and low levels of the set-up plan. The samples named from 33 to 37 in the most right of the graph are representing the mid-level parameter samples. Those samples are in this case ordered relatively tight to each other which indicate that the reproducibility of the response is good.

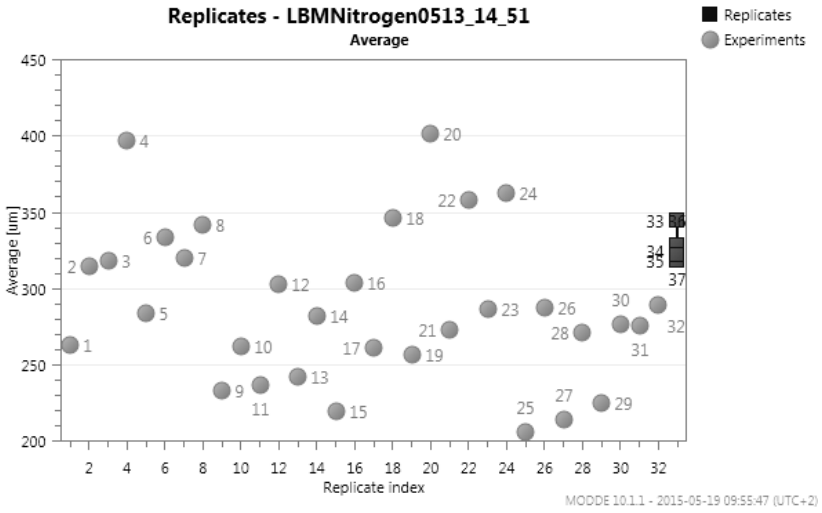

Figure 5. Replicate plot for the HAZ response showing the variation of HAZ among all sample of the Nitrogen series.

The summary of fit plot seen in figure 7 shows the model statistics of R2, Q2, model validity and model reproducibility for a particular response.

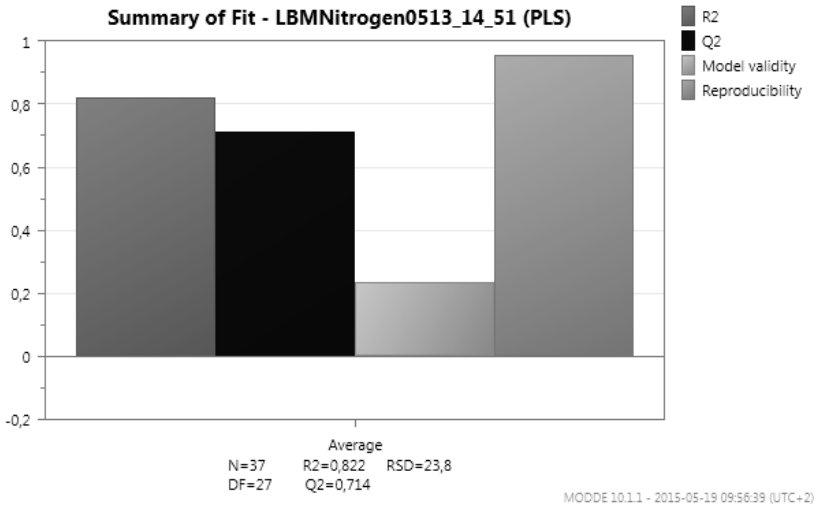

Figure 6. Summary of fit plot for the Nitrogen series. Average HAZ response showing R2, Q2, model validity and model reproducibility values.

In Modde a normal distributed response will in general lead to better model statistics and estimates. Almost all response from the Argon series was showing a positive skewness, which means that the peak of the distribution is located to the left of the mean output value. With a logarithmic transformation of the responses, the distribution appeared more as a typical normal distribution. An evidence of that this transformation worked was that the Q2, R2, regression and lack of fit in most cases were improved. The responses made from Nitrogen series appeared in most cases as normally distributed, no transformation was therefore needed.

To further optimize the model, a coefficient plot was produced which can be seen in figure 8. The coefficient plot presents regression coefficients relating to scaled and centered parameters together with the 95 % confidence interval. By excluding of parameters and interactions of parameters with low significance, Q2 was increased.

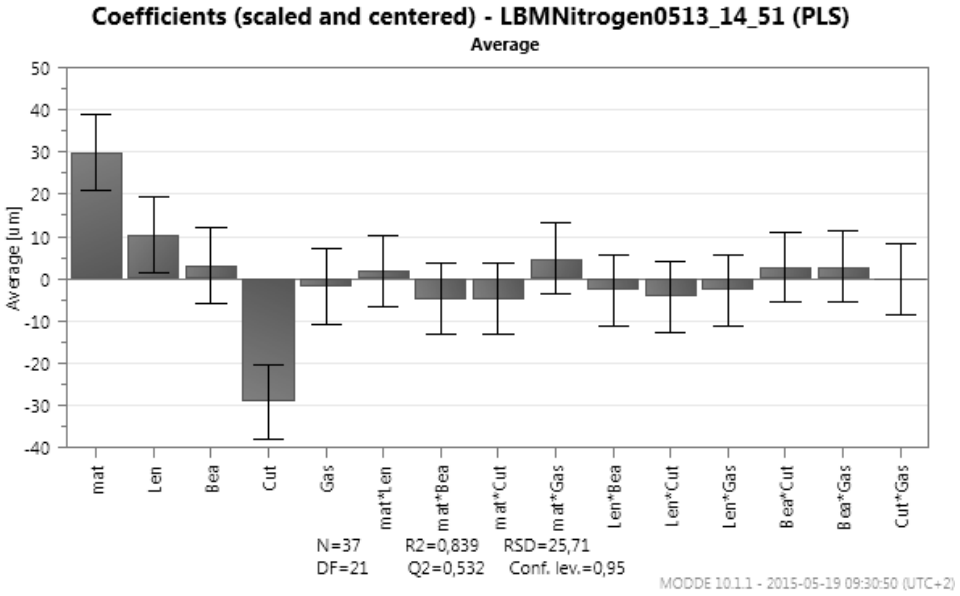

Figure 7. A non-optimized coefficient plot of the Nitrogen series average HAZ response. Removal of non-significant parameters such as the interaction parameters, gas pressure and beam power led to an increase of Q2.

4 Results

This chapter presents the result from the measurements carried out on the samples from the Argon and the Nitrogen series.

Figure 9 reveals the general difference between the cut surfaces with respect to assist gas. Two distinct zones can be observed on the 6,35mm Argon sample, one upper finer zone, and one lower zone which are more irregular and affected by heat. The lower irregular zone is also present on the 3,2mm Argon samples, while the 1mm Argon samples shows almost none of the lower irregular zone. The surfaces of the Nitrogen samples are more homogenous in its appearance, for all thicknesses. All the samples shows burr formation on the bottom side of the cut edge.

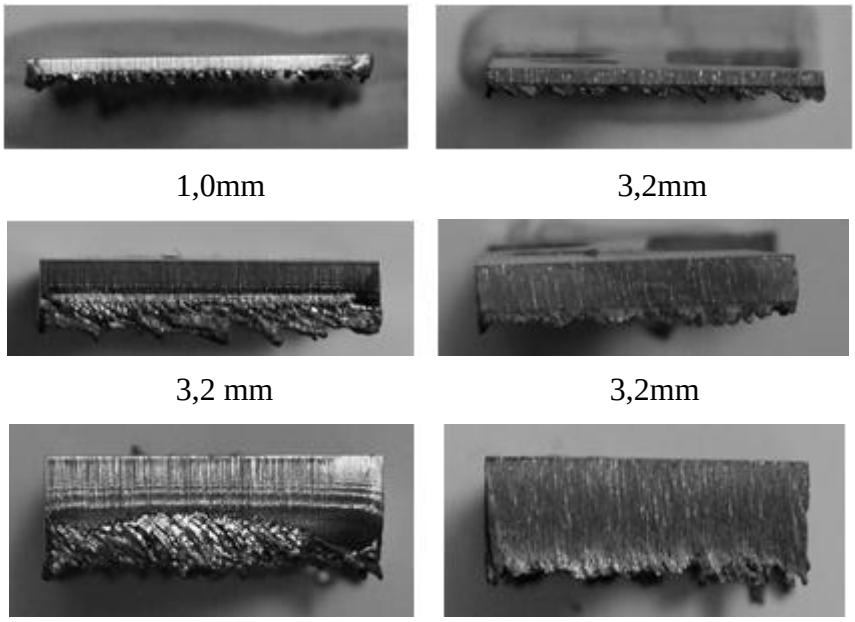

Figure 8. Examples of cut surfaces in different thicknesses with Argon used as assistant gas in a) and Nitrogen used as assistant gas in b).

4.1 Microstructure

The bulk microstructure of the Ti-6Al-4V sheet metal consists of mainly primary alpha and some beta which can be seen in figure 10.

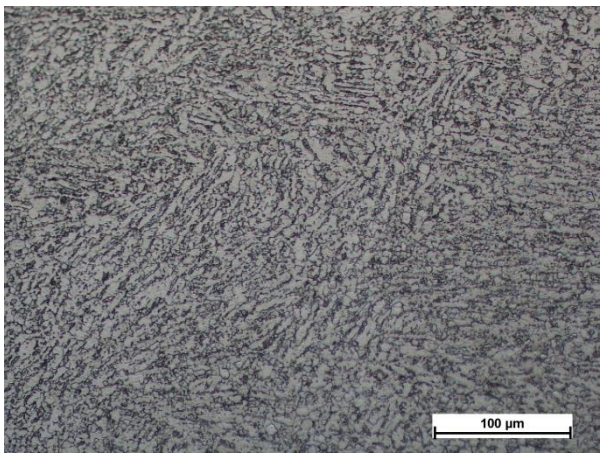

Figure 9. Light optical microscope image of the microstructure in the bulk material.

A picture of the microstructure at the cut edge on a longitudinal section can be seen in figure 11 for the Argon and Nitrogen series respectively. The structure is similar for both samples and consists of martensite in the HAZ. The microstructure of the samples cut with Nitrogen as assistant gas has a thin layer of alpha case at the most outer edge. The alpha case phase varies in size from mostly 4-5 µm wide but can be as large as 20 µm.

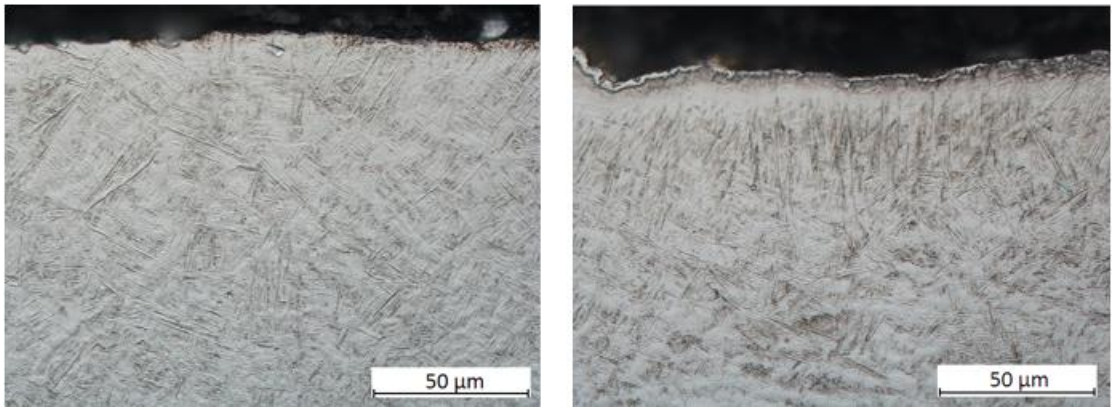

a) b)

Figure 10. Microstructure of sample cut with a) Argon and b) Nitrogen.

Further away from the cut edge less martensite appears in the HAZ and close to bulk material the martensite appears only as needles in a structure consisting of primary alpha in a beta matrix.

The transverse sections have a more irregular appearance as can be seen in figure 12. They are more affected by the heat and a variation of microstructures is observed in the surface. Even re-melted areas can be observed at the bottom edge in both the Argon and Nitrogen series. The Argon samples have a bigger area which is affected by the heat.

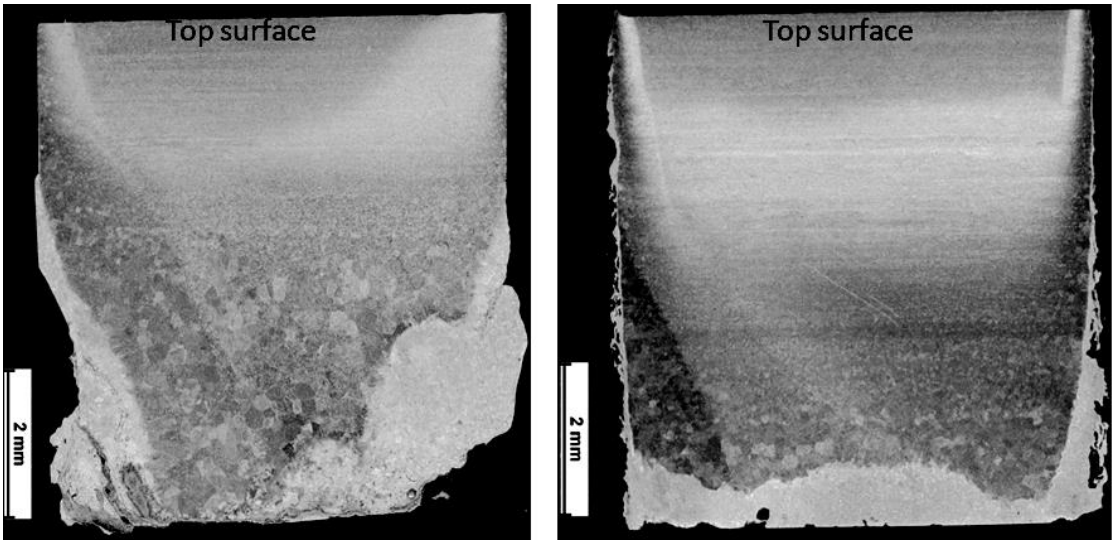

a) b)

Figure 11. Transverse section microstructure on a) Argon sample and b) Nitrogen sample.

4.2 HAZ

HAZ on the longitudinal sections have the same appearance and size for the Argon and Nitrogen series. The transverse sections differ in the sense that Argon samples exhibit a larger HAZ towards the bottom of the sample. The results from analysis in Modde are presented hereafter for the Nitrogen and Argon series.

4.2.1 Nitrogen series

Figure 13 shows model statistics for the longitudinal HAZ measurements on the Nitrogen series. The summary of fit plot shows a good R2 and Q2 value, meaning that the model is good and can predict the data in acceptable way. From the replicate plot it can be seen that the variability of the mid-level samples is small compared to the overall variability which indicates good reproducibility.

The longitudinal response shows a positive effect of increasing the material thickness, which means that if the material thickness is increased, HAZ will be increased. The cutting speed shows an equally big but negative effect on HAZ, a higher cutting speed leads to a smaller HAZ. Increasing the lens focal position has a positive effect on HAZ, a focus set deeper in the material leads to a larger HAZ.

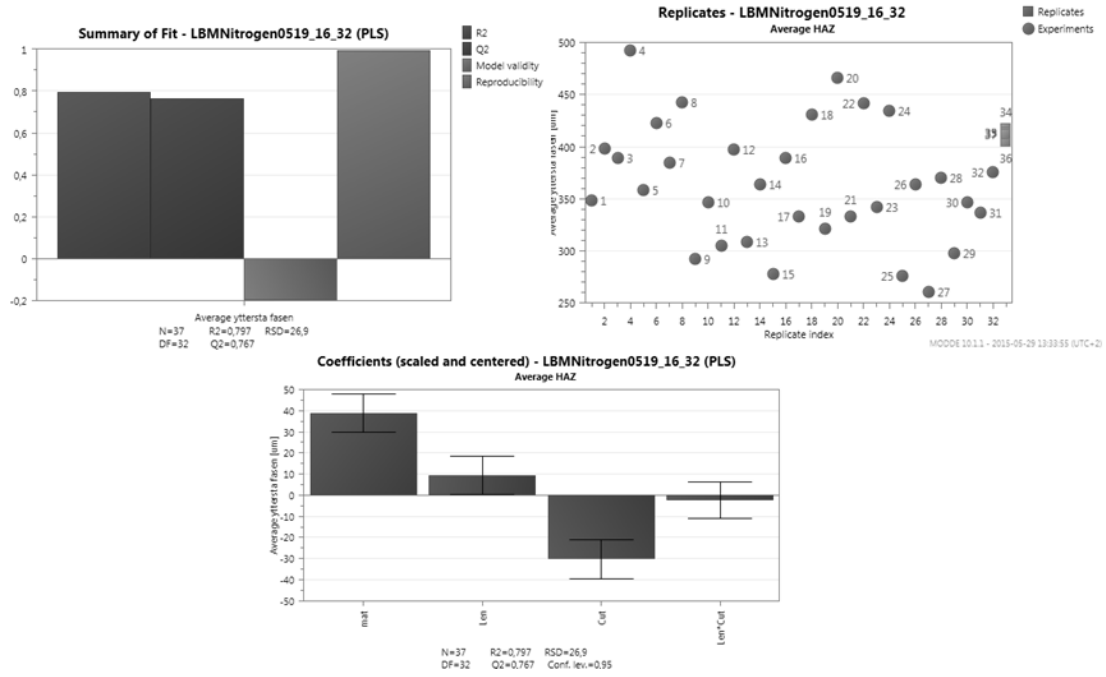

Figure 12. Summary of fit plot, replicate plot and coefficient plot for the longitudinal HAZ for the Nitrogen series.

The contour plot in figure 14 is showing the predicted response of HAZ when lens focal point and cutting speed are varying from their low to high value while the other cutting parameters are at their mid-level. As can be seen when changing cutting speed from 0,5mm/min to 1mm/min there is a decrease in HAZ of about 60 µm.

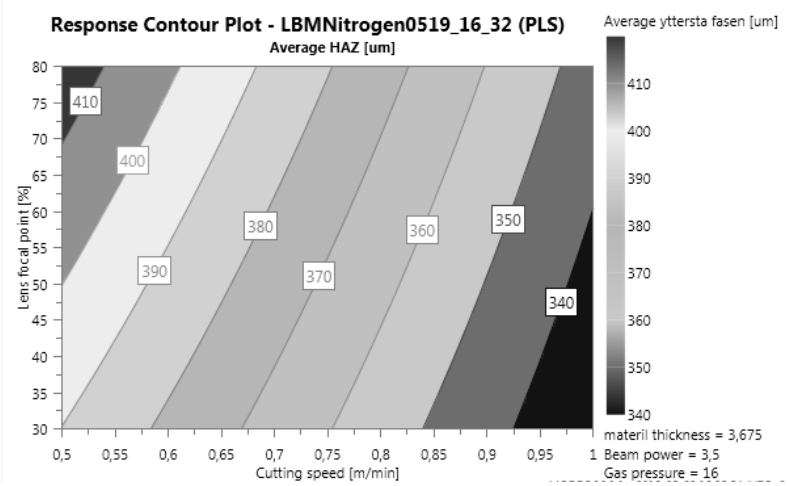

Figure 13. Contour plot showing the predicted effect of varying lens focal point and cutting speed on HAZ.

The effect of cutting speed and material thickness on the predicted value of HAZ can be seen in the contour plot in figure 15. HAZ is varying from 300 µm with high cutting speed and low material thickness, to 440 µm with low cutting speed at a higher material thickness.

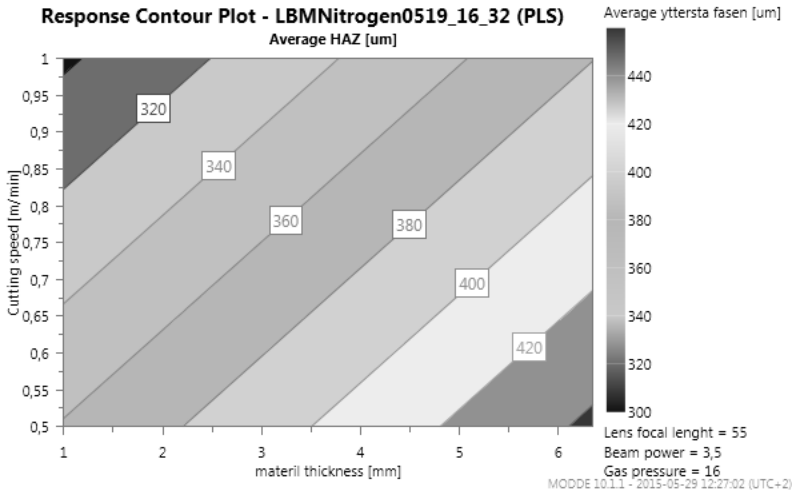

Figure 14. Contour plot showing the predicted effect of cutting speed and material thickness on HAZ.

Figure 16 shows model statistic for the transverse HAZ on the Nitrogen series. From the summary of fit plot and replicate plot it can be seen that the model fits the data in a good way and is able to predict new data and the reproducibility is good. The transversal response is revealing a somewhat different result compared to the longitudinal average response. The coefficient plot shows that cutting speed and gas pressure have a negative impact on HAZ, with cutting speed being the dominant factor. Lens focal point and beam power have a positive effect and results in increased HAZ.

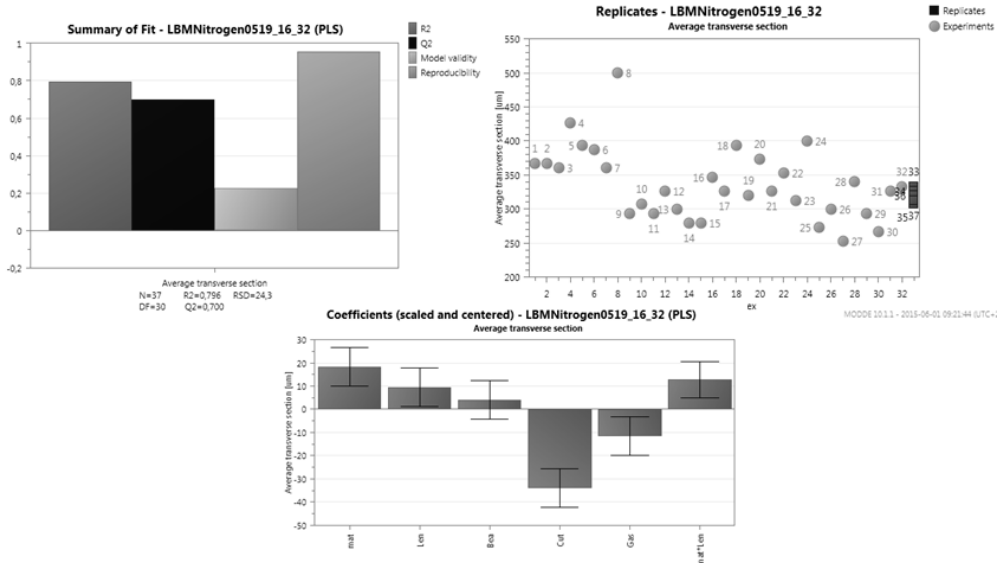

Figure 15. Summary of fit plot, replicate plot and coefficient plot for the transverse HAZ for the Nitrogen series.

The predicted effect on transversal HAZ is presented for material thickness and cutting speed in figure 17. HAZ is varying from around 280 µm for high cutting speed and low material thickness to 380 µm for low cutting speed and a high material thickness.

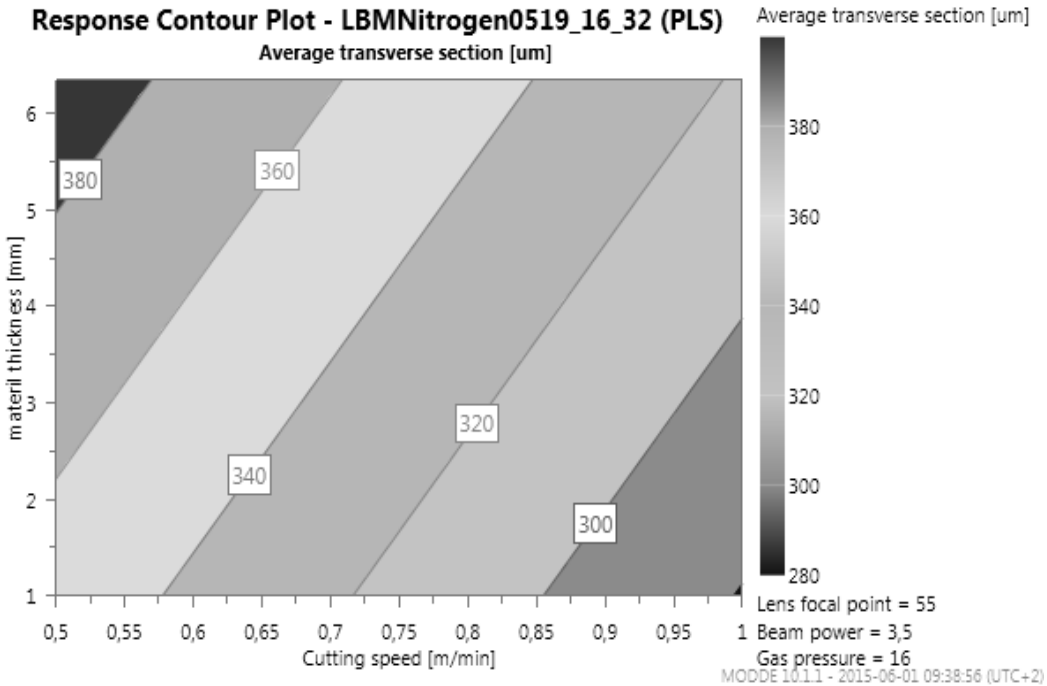

Figure 16. Contour plot showing the predicted effect of varying material thickness and cutting speed on the HAZ.

4.2.2 Argon series

Figure 18 shows the summary of fit plot, replicate plot and coefficient plot for the HAZ measurements made on the longitudinal section. From these plots it can be seen that the R2 and Q2 values are good and the reproducibility of the test is good.

The effect of varying various parameters on HAZ can be seen in the coefficient plot in figure 18. From the graph it can be seen that cutting speed and gas pressure have a negative effect on HAZ with cutting speed being the dominant factor. Increased cutting speed and gas pressure results in that HAZ is decreased. Beam power has a positive effect meaning that increased beam power leads to increased HAZ values.

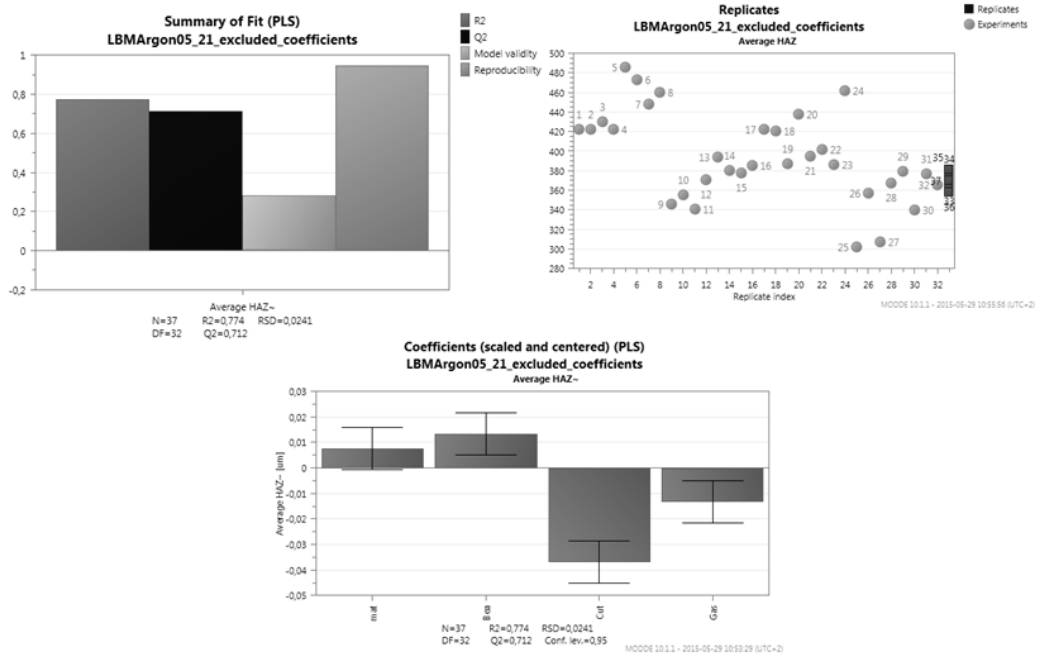

Figure 17. Summary of fit plot, replicate plot and coefficient plot for HAZ on the longitudinal section for the Argon series.

The predicted HAZ is presented for cutting speed and gas pressure in figure 19. HAZ is varying from 350 µm for high cutting speed and high gas pressure, to 430 µm for low cutting speed and low gas pressure.

The contour plot in figure 20 shows the predicted effect of cutting speed and beam power on HAZ. The same variation as in figure 20 can be observed where cutting speed is the dominant factor.

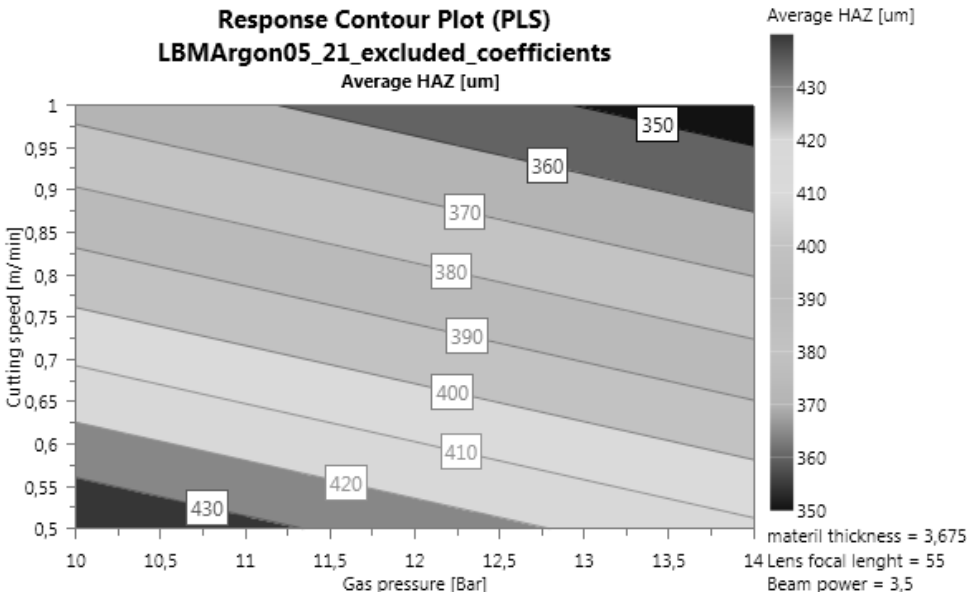

Figure 18. Contour plot showing the predicted effect of cutting speed and gas pressure on HAZ.

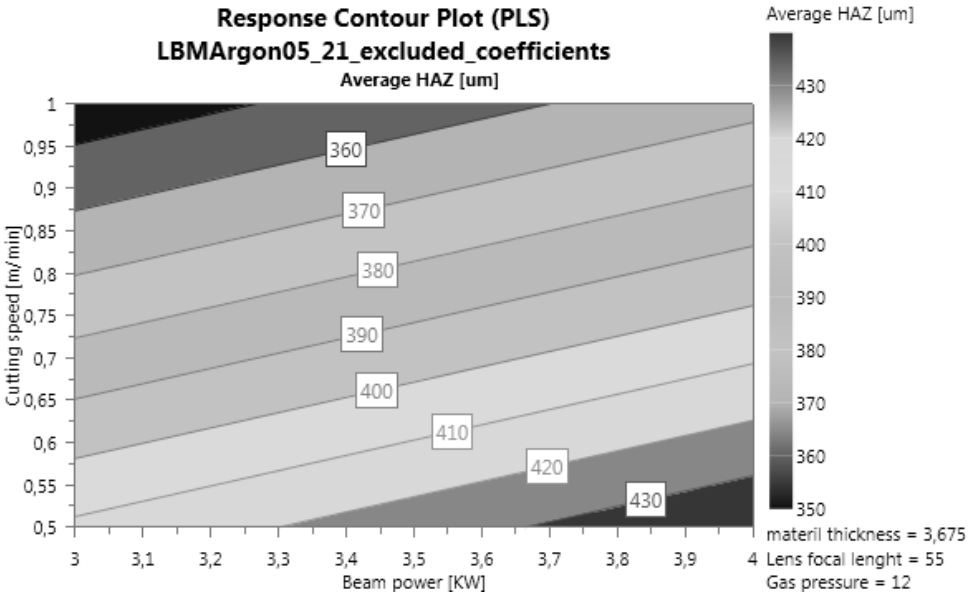

Figure 19. Contour plot showing the predicted effect of cutting speed and beam power on HAZ.

The statistics for the transverse sections are presented in figure 21. The summary of fit plot reveals that the model has a Q2 value that is half of what is acceptable and also R2 and reproducibility are a little bit below their limit values. Therefore, no emphasis can be placed on the effects shown in the coefficient plot.

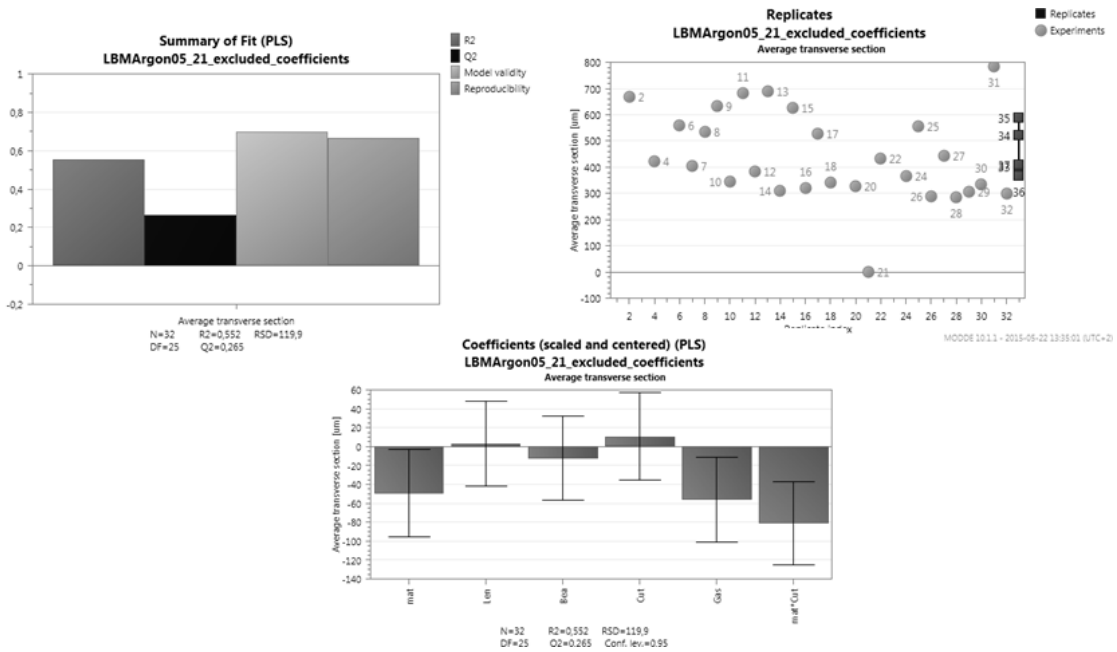

Figure 20. Summary of fit plot, replicate plot and coefficient plot for HAZ on the transverse section for the argon samples

4.3 Burr

The properties of the Burr differed between the Argon and Nitrogen series. The burr of the Argon samples are more irregular in its appearance as can be seen in figure 9, chapter 4. The maximum height did not differ between the two series.

The maximum burr height was measured on the Argon and Nitrogen series. The summary of fit plot, replicate plot and coefficient plot for maximum burr height can be seen in figure 22 and 23 for the Argon and Nitrogen series respectively. From the replicate plot in figure 22 it can be seen that the measured burr height on the samples cut with mid-level parameter settings is higher than the majority of the other samples. The resulting model has therefore bad fit with the data and the ability to predict new data is low as seen in the summary of fit plot.

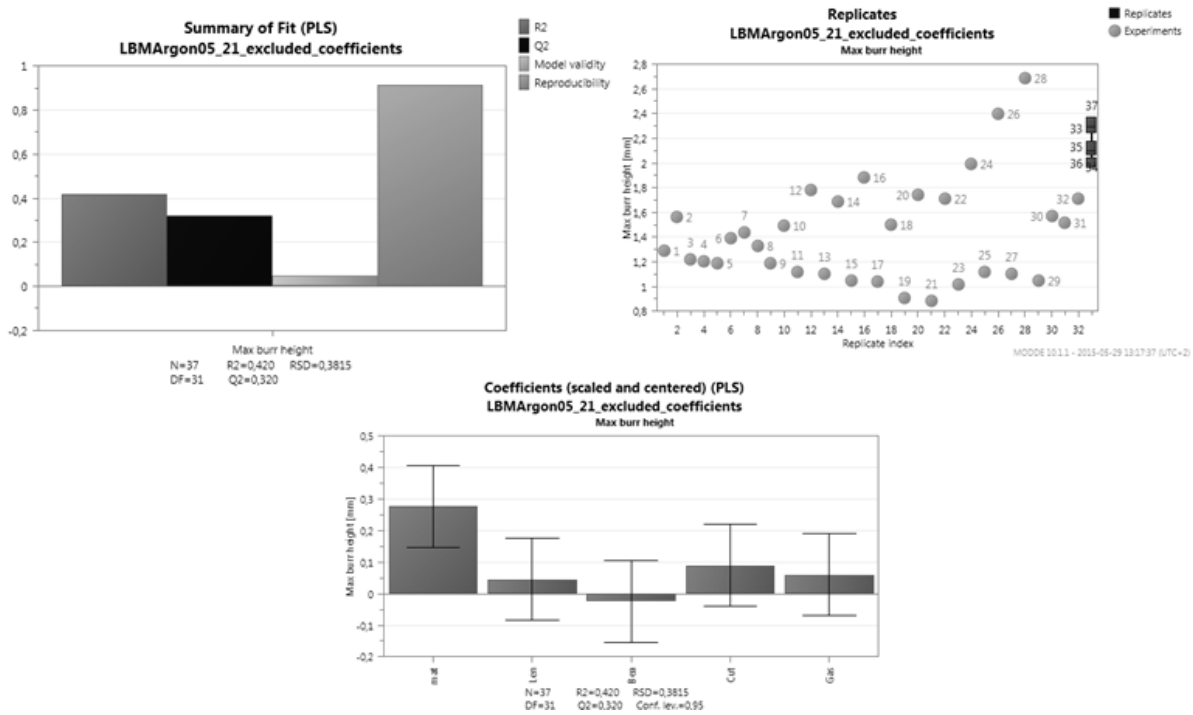

Figure 21. Summary of fit plot, replicate plot and coefficient plot of the maximum burr height for the Argon series.

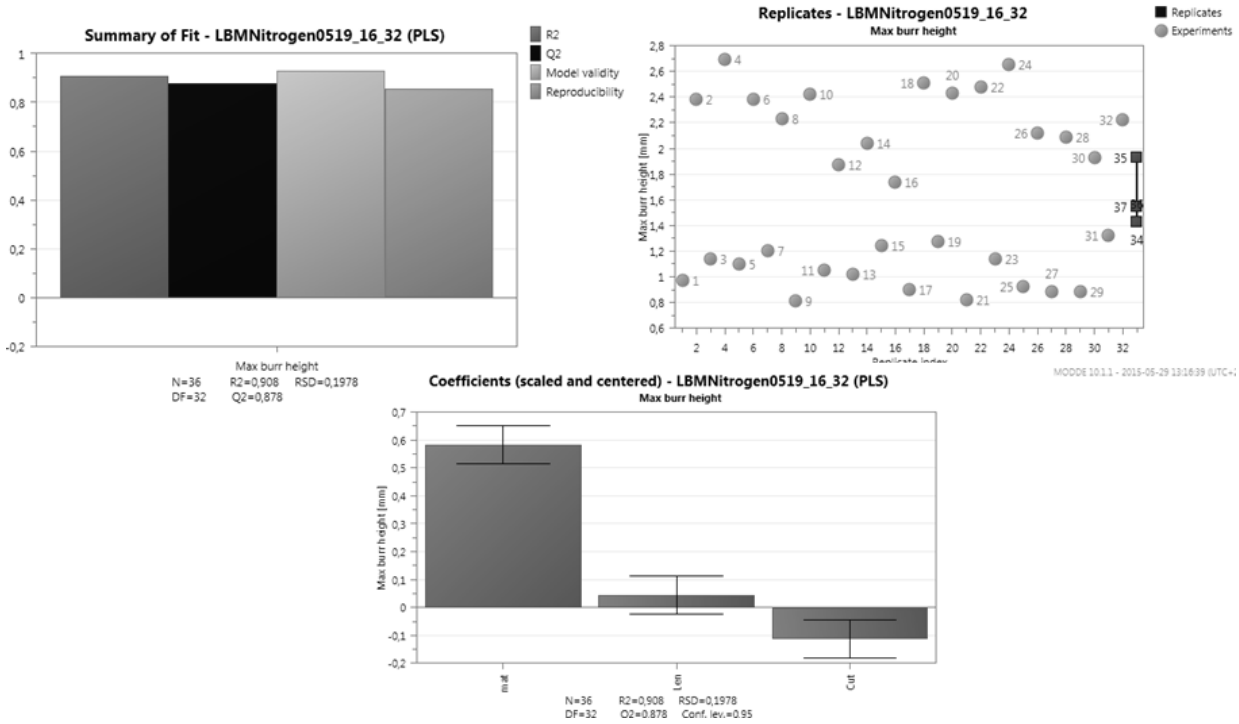

Figure 22. Summary of fit plot, replicate plot and coefficient plot of the maximum burr height for the Nitrogen series.

The model prediction of maximum burr height for the Nitrogen samples is shown in the contour plot in figure 24 for cutting speed and material thickness. From the plot it

can be seen that the biggest effect on burr height comes with change in material thickness.

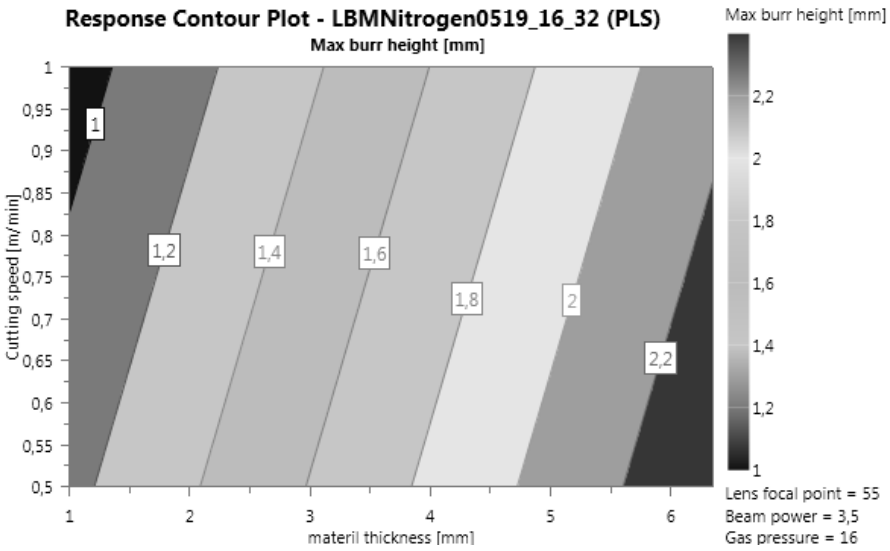

Figure 23. Contour plot showing the predicted effect of varying cutting speed and material thickness on maximum burr height.

4.3.1 Burr classification

The nylon brush was insufficient for removing the burrs on the 6,35 mm samples. It should be pointed out that this material is not what should be considered as regular burrs like in conventional machining but re-melted material from the cutting process. The result after deburring the 3 mm samples differed with respect to assist gas. Only little material was removed from the Argon sample whilst the Nitrogen sample showed a smooth edge with a small chamfering. The 1 mm samples burrs could be deburred with much less effort, especially the Nitrogen samples which showed a more brittle type of burrs. The test resulted in that the burr was classified according to table 6.

Table 6. Classification of burrs present on the Nitrogen and Argon series.

Thickness and assistant gas	class
1mm Nitrogen	1
1mm Argon	2
3.2 mm Nitrogen	3
3,2 mm Argon	4-5
6,35 mm Argon and Nitrogen	4-5

4.4 Surface irregularity

The surface irregularity differed with respect to assist gas. The Nitrogen samples revealed an average surface irregularity that is 10 times larger than of the Argon samples, as can be seen in table 7.

Table 7. Surface irregularity statistics for both the Argon and Nitrogen series.

	Argon	**Nitrogen**
Average [um]	4	40
Standard deviation [um]	2	11
Maximum[um]	20	100
Minimum[um]	2	10

Analyze of the Nitrogen series surface irregularities was not possible in Modde because of poor reproducibility, bad model fit and insufficient ability to predict variation.

Figure 25 shows the summary of fit plot, replicate plot and coefficient plot for surface irregularity on the Argon samples. The figure indicates a good model that fits and predicts the data together with a good reproducibility. From the coefficient graph it can be seen that material thickness and beam power both affect surface irregularity in a positive way, meaning that when material thickness and beam power increases from their average- to high value, surface irregularity is increasing.

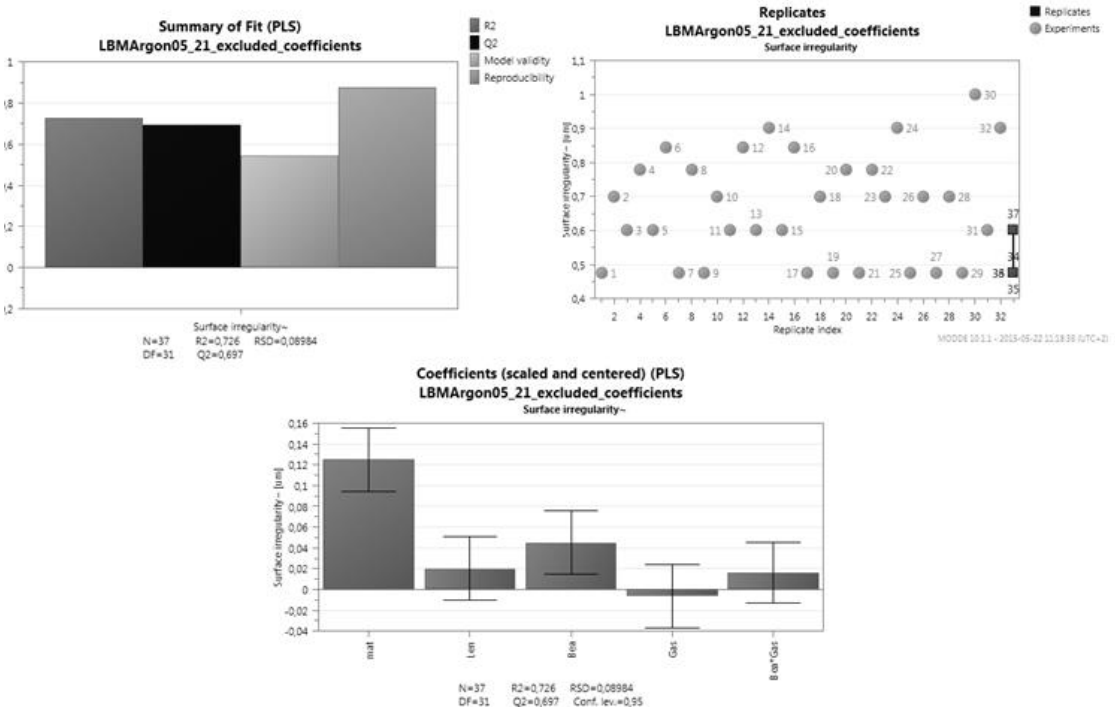

Figure 24. Summary of fit plot, replicate plot and coefficient plot for the surface irregularity for the Argon series.

The contour plot in figure 26 is showing the effect on surface irregularity when beam power and material thickness is varied. From the plot it can be seen that material thickness has the largest effect on surface irregularity.

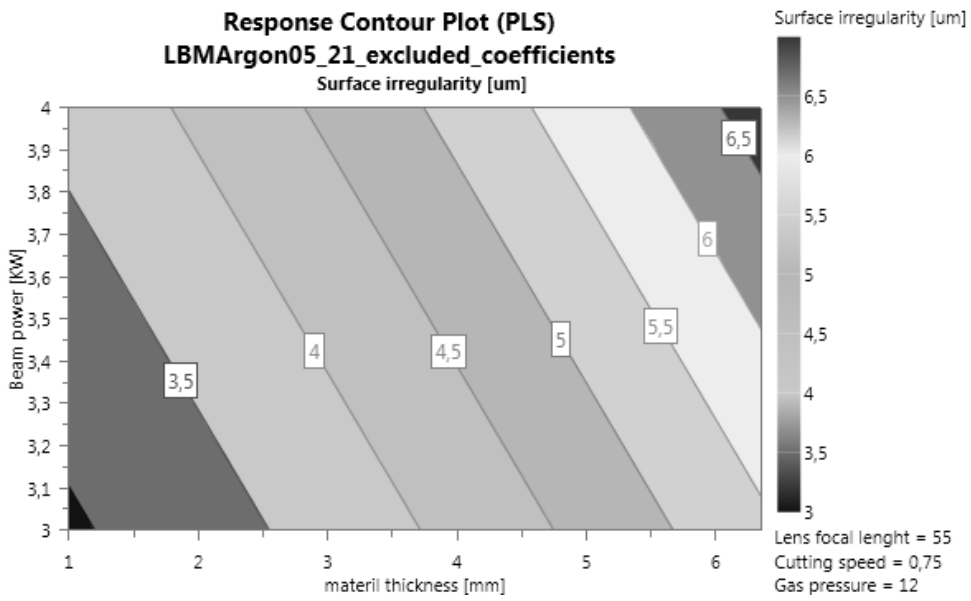

Figure 25. Contour plot showing the predicted effect of beam power and material thickness on surface irregularity for the Argon series.

4.5 Hardness measurements

The hardness measurements are presented below. The measurements made on the transversal sections is presented in graphs which differs in material thickness and assistant gas used. The hardness measured on the longitudinal sections is presented with average values from all the thicknesses.

The hardness on the 6,35 transverse sections has values that are 2-3 times higher than the bulk material, both for the Argon and Nitrogen sample. As shown in the graphs in figure 27 and figure 28, the hardness is highest at the bottom of the sample and is decreasing towards the top and evens out at around 400 Vickers at approximately 2 mm from the top on the Argon samples. The high hardness values for the Nitrogen samples do not extend as far towards the top as for the Argon samples.

In figure 29 it can be seen that the hardness of the 3,2 mm Argon sample is around 400 HV near the cut edge and is decreasing to bulk value at a distance of 200 µm from the edge. The higher hardness extends further in from the edge at the bottom of the sample.

The 3,2 mm Nitrogen sample have peak values of 550-750 HV near the cut edge as seen in figure 30. The hardness is above 400 HV and is decreasing towards bulk hardness at a distance of 250 µm from the cut edge. No drop in hardness is observed at the bottom of the sample.

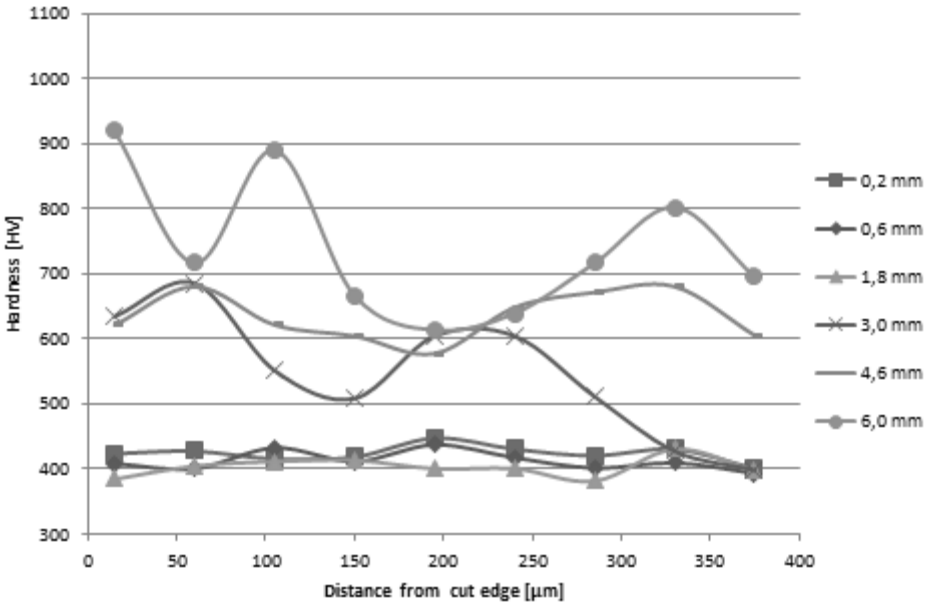

Figure 26. Hardness measurements on a transvers section of 6,35 mm Argon sample.

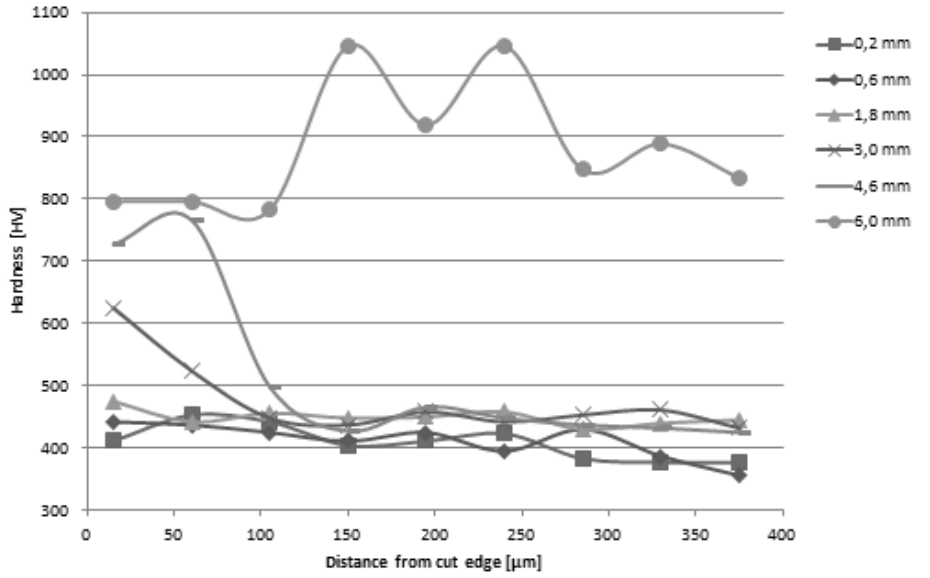

Figure 27. Hardness measurements on transvers section of 6,35 mm Nitrogen sample.

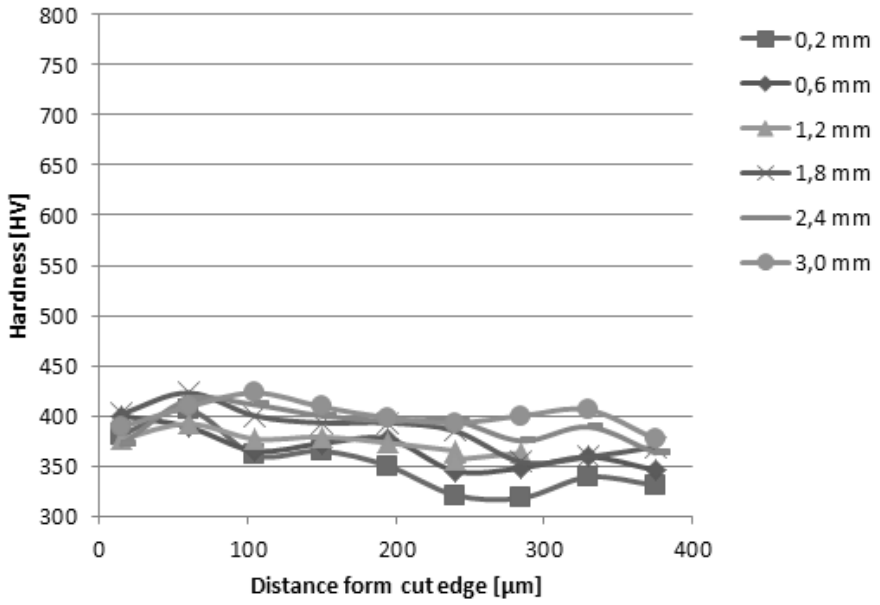

Figure 28. Hardness measurements on a transverse section of 3,2 mm Argon sample.

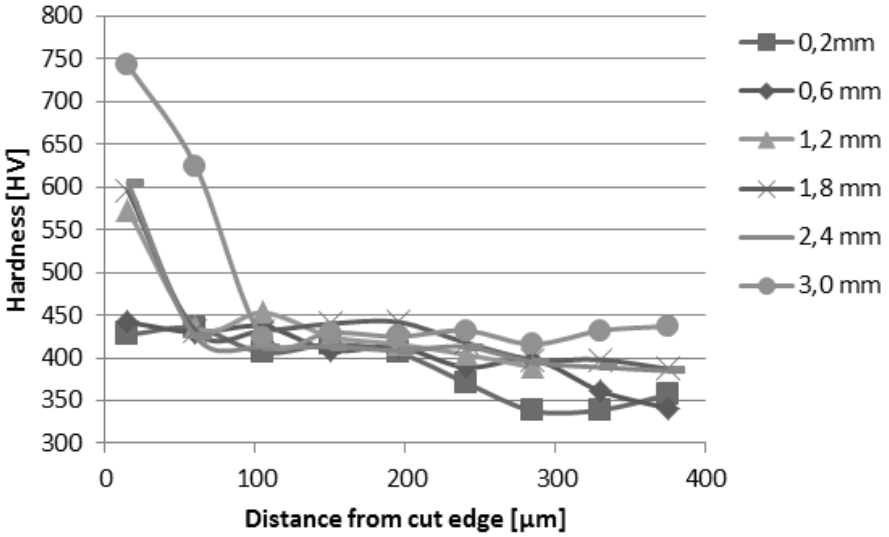

Figure 29. Hardness measurements on a transverse section of 3,2 mm Nitrogen sample.

In figure 31 it can be observed that the 1 mm transverse Argon samples have uniform hardness throughout the thickness. The 1 mm transverse Nitrogen sample shows higher hardness near the cut edge as seen in figure 32. Hardness starts to decrease at around 200 µm and is reaching bulk values 350µm from the cut edge.

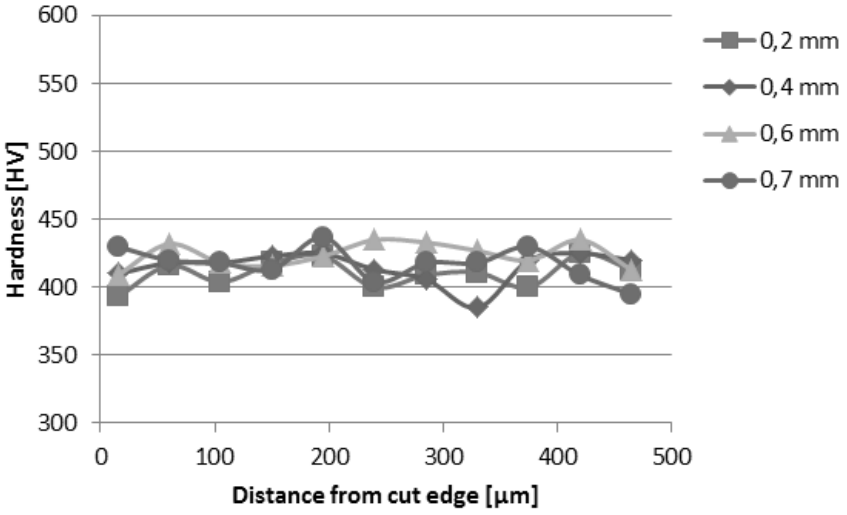

Figure 30. Hardness measurements on a transverse section of 1,0 mm Argon sample.

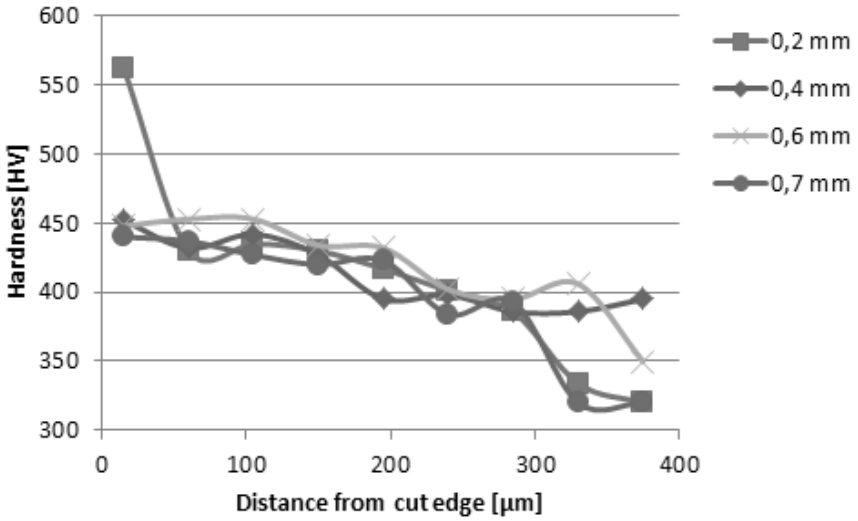

Figure 31. Hardness measurements on a transverse section of 1,0 mm Nitrogen sample.

The hardness measurements from the Argon longitudinal sections can be seen in figure 33. The hardness is decreasing linearly towards its bulk value at approximately 400 µm from the edge. A small dip in hardness is observed near the cut edge.

Peak value of the hardness can be observed in figure 34 on the Nitrogen longitudinal section. The hardness is decreasing and is reaching bulk values at around 350 µm from the cut edge.

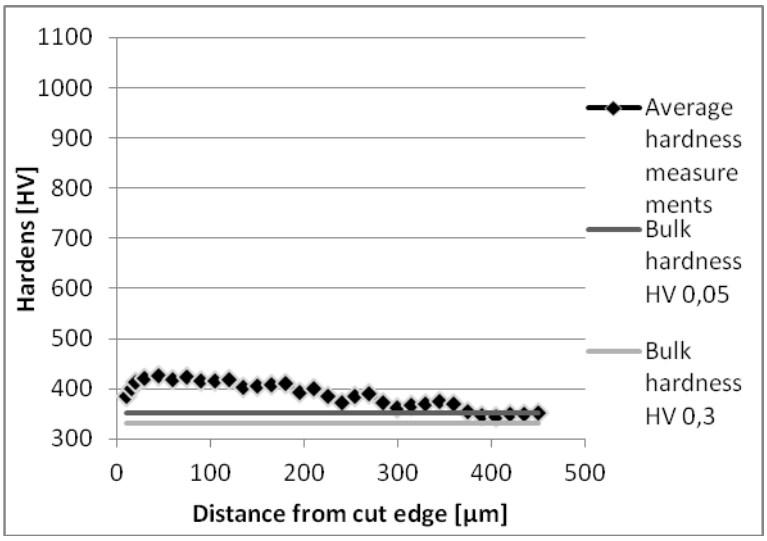

Figure 32. Hardness measurements on a longitudinal section of a 1,0 mm Argon sample

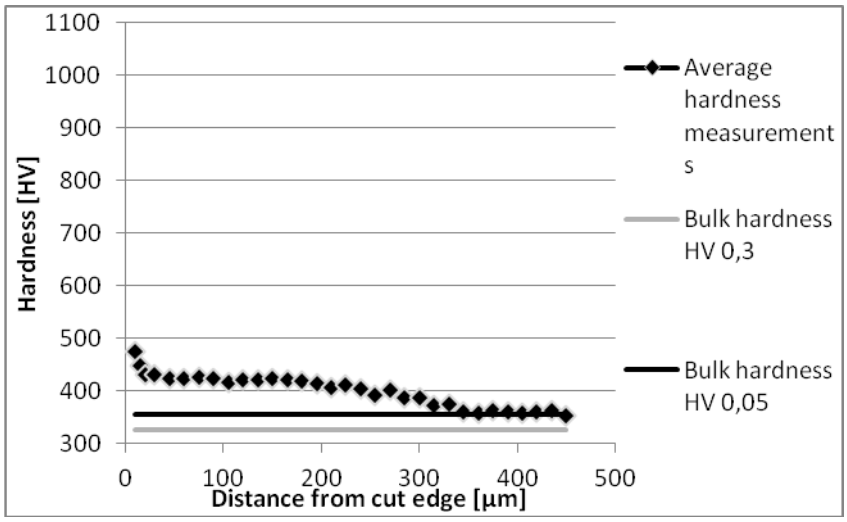

Figure 33. Hardness measurements on a longitudinal section of a 1,0 mm Nitrogen sample.

5 Discussion

5.1 Microstructure

Closest to the cut edge in the HAZ, the microstructure consists of mainly martensite on both the Argon and Nitrogen longitudinal sections. This structure reveals that a high cooling rate has been present.
The alpha-case phase present on the Nitrogen samples at the most outer edge of the HAZ can be explained by that the Nitrogen of the assistant gas has stabilized alpha. Nitrogen is according to Leyens and Peters (2003) a strong alpha stabilizer.

The microstructure on the transverse sections is hard to characterize since it is so irregular in its appearance. It changes shifts from martensite at the top, to a recrystallized Widmanstätten type of structure and then remelted material. This indicates a higher cooling rate at the top which then decreases towards the bottom of the sample.

5.2 HAZ

The Nitrogen series and the Argon series show some differences in their response to varying some of the parameters. The cutting speed revealed a negative effect on HAZ for both the Nitrogen and the Argon series, this negative effect is in line with what Shanjin & Yang (2006) and Tirumala Raoa et al. (2005) has presented. The cutting speed proved to be the parameter with the greatest impact on the HAZ in this set-up.

One can easily believe that an increase of material thickness would make the HAZ smaller since there is more material surrounding the hot area that could conduct away heat energy. This theory is valid in a welding context, since the heat input is the same no matter the material thickness. In Laser cutting this is not valid since a thicker material would lead to a larger contact zone of the laser beam and hence an increase of heat input and therefore also a larger HAZ. As seen in figure 13 in section 4.2.1, a greater material thickness leads to a larger HAZ. This result differs between the Nitrogen and Argon series. The HAZ on the longitudinal Argon samples exhibit only a small positive effect of increasing the material thickness. A possible explanation for the difference response of Argon and Nitrogen samples when varying material thickness could be the different inherent properties of the respective gas.

Some differences of how the gas pressure is affecting the HAZ can be noted. The longitudinal Argon series and the transversal Nitrogen series show a negative effect while the longitudinal Nitrogen series reveal no effect of varying the gas pressure. A negative effect is in line with results presented by Shanjin & Yang (2006). A possible reason for the inconsistent result might be a too small difference between the low and the high level of the gas pressure.

The beam power does also reveal differences between the Argon series and the Nitrogen series. The longitudinal sections of the Nitrogen series show no effect of varying beam power while the transversal sections of the Nitrogen samples and the

longitudinal Argon samples show a positive effect. A positive effect on HAZ when increasing the beam power is in line with results by Shanjin & Yang (2006) and Teixidor et al. (2014).

The varying of the lens focal point also shows inconsistent results. The HAZ of the Nitrogen series reveals a positive effect of setting the lens focal point deeper into the material while the HAZ of the Argon series is not showing a variation of the focal position. However, the effect of varying the focal position is small on the Nitrogen samples and not significant on the Argon samples. This indicates that the effect on HAZ when varying focal position is small or non-existent.

5.3 Hardness

The high hardness of the 6,35 mm thick Argon and Nitrogen samples measured on the transversal sections can be correlated to the microstructure in the cut surface. As can be seen in figure 9, chapter 4. The transverse cut surface differs in appearance with respect to the two gases. The two distinct zones observed on the 6,35 thick Argon sample seen in figure 9 in chapter 4 can be correlated to the hardness values in figure 27, section 4.5. The hardness measurements located 0,2, 0,6 and 1,8 mm from the upper surface is within the finer zone of the surface. The hardness in those three locations is around 400 HV, which indicates martensitic structure according to Leyens & Peters (2003). The high values of 500-900 HV observed in the lower zone are more difficult to link to a specific microstructure, but when observing figure 12 in section 4.1, one can see a clear difference compared to at the top surface. New grains have started to grow which indicates slower cooling compared to with the top surface. The increase of hardness might come from dissolved atmospheric elements like Oxygen and Nitrogen that take interstitial spots in the crystal structure and hence the hardening effect. In general, the microstructure in the lower zone is irregular and hard to characterize.

The hardness values on the samples cut with Nitrogen as assist gas can be seen in figure 28, section 4.5. The hardness measurements made 0,2 , 0,6 and 1,8 mm from the top surface exhibit the same behavior as on the Argon transverse section, with the difference that higher hardness is observed closer to the cut edge. The high values can be linked to the alpha case phase present on the Nitrogen samples. This is in line with what Gurappa (2003) presented when cutting in Titanium with Nitrogen as assist gas. He found that alpha-case causes an increased hardness in the area of the cut edge. This phase varies in thickness from 0 to 20 µm and has a Vickers hardness of over 800 HV.

Alpha case has caused irregularities in the hardness measurements. Since the indent is approximately 15 µm wide and the alpha case varies between 0 and 20 µm, the indents closest to the edge have in some cases been placed in the alpha case. Furthermore, in the lower zone of the nitrogen sample, it can be observed that the higher hardness is not present as far into the material as for the Argon samples. This may be correlated again to the difference between the appearances of the cut surface, where Argon samples seem to be more affected by the heat.

The transverse section on the 3,2 mm Nitrogen samples have peak hardness at the outer most edge reaching values above 700 HV. As for the 6,35 mm samples those values are likely to be correlated to alpha-case. The transverse section on the 3,2 mm Argon sample has uniform hardness throughout the thickness. The absence of the extreme hardness values observed on the 6,35 mm samples can be explained by that the cut surface is lacking the lower irregular zone mentioned earlier. Instead the cut surface is uniform and clean in appearance. The hardness is indicating martensitic structure.

The hardness of the longitudinal sections on Argon and Nitrogen samples differ with respect to the first 30 µm. In this area, Argon samples exhibit a drop in hardness while Nitrogen shows peak values. The drop in hardness for the Argon samples may be due to that the indent have caused the edge to bulge because there is no metal to resist the deformation which resulted in an inaccurate depression and thus in an incorrect hardness value. The peak values on the Nitrogen samples are within the area where alpha-case is present and can thus be explained by that.

5.4 Burr

Nitrogen samples showed burrs which were regular in its appearance over the whole sample. The burr on the Nitrogen samples where more brittle compared to the Argon samples which resulted in that Nitrogen samples were placed in a lower class based on how difficult it was to remove the burr. The reason for the brittleness is not quite clear. When cutting in Titanium, Argon act as an inert gas and Nitrogen does not. Hence, it is quite likely that Nitrogen will diffuse in, and react with the material during the cutting process. Evidence of that this has happened on the samples cut with Nitrogen in this experiment is the yellow surface observed. This is in line with what Tirumala Raoa et al. (2005) presented when cutting with Nitrogen in Titanium. The yellow surface indicates presence of TiN which is brittle in its nature and leads to a more brittle type of burr. Hence, the burr on the Nitrogen samples is easier to remove than the burr on the Argon samples.

Burr height measurements on the samples cut with Argon as assist gas showed poor values of R2, Q2 and model validity. These poor values originates from the 3,2 mm mid-level samples, they have a burr height that were in the top range of the results which can be seen in the replicate plot in figure 22 in section 4.3. This is the main reason for the bad model statistics. Another reason could be that the peaks were random over the sample and few in number.

The burrs observed on the 6,35 mm samples and 3,2 mm samples cut with Argon is not something seen in regular production where a class 3 type of burr, which can be removed with an abrasive nylon wheel, is the maximum tolerated. If higher classes are observed then focus are on finding the root cause to it, rather than accept it and machine it away.

5.5 Surface irregularity

The surface irregularity measurements of the Nitrogen samples showed bad model statistics. The measurements method of selecting the biggest irregularity in the field of view in the microscope proved to be too irregular to be able to be used on such big irregularities like the Nitrogen samples. However, the Argon samples showed good model statistics and lead therefore to results that could be determined as valid. The reason for the big difference in surface irregularities between the Argon and Nitrogen series could be because by inertness of Argon. This is in line with what Davim (2013) have shown, that cutting with Argon produces finer surfaces.

6 Conclusions

- HAZ, surface irregularity and burr height increase with increased material thickness for the process parameters used in this study.
- Cutting speed should be maximized to reduce HAZ.
- The Nitrogen samples showed greater surface roughness compared to the Argon samples.
- Subsequent machining is needed when cutting with Nitrogen as assist gas to remove the alpha-case.
- HAZ exhibits increased hardness compared to bulk material. Hardness can be correlated to the microstructure.

6.1 Further research recommendations

Make experiments on a specific material thickness, to be able to test with wider process parameter ranges in order to see greater variations in the responses. Examples of the process parameters to increase the range of could be cutting speed, beam power and gas pressure.
Preform laser cutting in titanium sheet with both Fiber and CO_2 laser to see if there could be any advantages of utilization of either of those.
It was noted during the evaluation of the extra samples that an increase of cutting speed resulted in a surface which were less heat affected and thereby a surface that showed smaller lower zone with more irregular structure. Further studies of those samples might provide even other useful information regarding cutting with higher speeds.
Measuring the surface irregularities with a stylus profilometery might improve the quality of the surface irregularity measurements. Better quality of those measurements could than yield better statistical evaluation and thereby greater understanding of the process parameters effect on surface irregularities.

7 Bibliography

Almeida, L. o.a. 2006. Optimization of titanium cutting by factorial analysis of the pulsed nd:yag laser parameters. *Journal of Materials Processing Technology,* Vol. 179, pp. 105-110.

Anon., 2015. *The Linde Group.* [Online]
Available at: http://www.linde-gas.com/en/processes/cutting_joining_and_heating/cutting/laser_cutting/laser_cutting_with_nitrogen/index.html
[2 June 2015].

Aurich, J. o.a., 2009. Burrs-Analysis, control and removal. *Springer-Verlag Berlin and Heidelberg GmbH & Co. KG.*

Boyer, R., Welsch, G. & Collings, E., 1994. *Materials Properties Handbook - Titanium Alloys.* 2 red. u.o.:ASM International.

D.A. Porter, K. E. M. S., 2009. *Phase Transformations in Metals and Alloys.* 3rd red. u.o.:u.n.

Davim, J. P., 2013. *Nontraditional Machining Processes: Research Advances.* u.o.: Springer Science & Business Media.

Ezugwu, W. & Wang, Z., 1997. Titanium alloys and their machinability - a review. *Journal of Materials Processing Thechnology,* Vol. 68, pp. 262-274.

Gurappa, I., 2003. Prediction of titanium alloy component life by developing. *Journal of Materials Science Letters,* Vol. 22, pp. 771-774.

Karatas, C., Keles, O., Uslan, I. & Usta, Y., 2006. Laser cutting of steel sheets: Influence of workpiece thickness and beam waist position on kerf size and stria formation. *Journal of Materials Processing Thechnology,* Vol. 71, pp. 22-29.

Leyens, C. & Peters, M., 2003. *Titanium and titanium alloys: fundamentals and applications.* u.o.:Wiley-VCH.

Pandey, A. & Dubey, A., 2012. Simultaneous optimization of multiple quality characteristics in laser cutting of titanium alloy sheet. *Optics and Laser Thechnology,* Vol. 44, pp. 1858-1865.

Powell, J., 1998. *C02 laser cutting.* u.o.: Springer-Verlag London Limited.

Scintilla, L., Palumbo, G., Sorgente, D. & Tricarico, L., 2013. Fiber laser cutting of Ti6Al4 sheets for subsequent welding operations: Effect of cutting parameters on butt joints mechanical properties and strain behaviour. *Material & Design,* Vol. 47, pp. 300-308.

Semiatin, S., 2010. *Metalworking: Sheet Forming.* 14B red. u.o.:ASM International.

Shanjin, L. & Yang, W., 2006. An investigation of pulsed laser cutting of titanium alloy sheet. *Optics and Lasers in Engineering,* Vol. 44, pp. 1067-1077.

Steen, W. & Mazumder, J., 2010. *Laser Material Processing.* u.o.: Springer-Verlag London Limited.

Teixidor, D., Ciurana, J. & Rodriguez, C., 2014. Dross formation and process parameters analysis of fibre laser cutting of stainless steel thin sheets. *International Journal of Advanced MAnufacturing Thechnology,* Vol. 71, pp. 1611-1621.

Thombansen, U., Hermanns, T. & Stoyanov, S., 2014. Titanium and titanium alloys. *ASM HAndbook Processing, and Structure on Properties of Nonferrous Alloys,* Vol. 20, pp. 98-102.

Tirumala Raoa, B., Kaul, R., Tiwara, P. & Nath, A., 2005. Inert gas cutting of titanium sheet with pulsed mode CO2 laser. *Optics and Lasers in Engineering,* Vol. 43, pp. 1330-1348.

Weber, M., 1999. *Handbook of Laser Wavelengths.* u.o.:CRC Press LLC.

Voort, V. & George, F., 2004. *ASM Handbook: Metallography and microstructures.* u.o.: ASM International.

8 Appendix

8.1 Appendix A: Experimental test set-up

A1: Experimental set-up for the samples cut with Argon as assist gas.

Table 1A. Test plan showing the different parameter levels used.

Mount no	Exp No	Exp Name	Run Order	Material thickness	Lens focal	Beam power	Cutting speed	Gas pressure
15-0239-M-001	1	1A	1	1	30	3	0,5	10
15-0239-M-002	2	2A	32	6,35	30	3	0,5	10
15-0239-M-003	3	3A	16	1	80	3	0,5	10
15-0239-M-004	4	4A	25	6,35	80	3	0,5	10
15-0239-M-005	5	5A	30	1	30	4	0,5	10
15-0239-M-006	6	6A	24	6,35	30	4	0,5	10
15-0239-M-007	7	7A	28	1	80	4	0,5	10
15-0239-M-008	8	8A	31	6,35	80	4	0,5	10
15-0239-M-009	9	9A	26	1	30	3	1	10
15-0239-M-010	10	10A	34	6,35	30	3	1	10
15-0239-M-011	11	11A	4	1	80	3	1	10
15-0239-M-012	12	12A	10	6,35	80	3	1	10
15-0239-M-013	13	13A	14	1	30	4	1	10
15-0239-M-014	14	14A	36	6,35	30	4	1	10
15-0239-M-015	15	15A	8	1	80	4	1	10
15-0239-M-016	16	16A	9	6,35	80	4	1	10
15-0239-M-017	17	17A	29	1	30	3	0,5	14
15-0239-M-018	18	18A	12	6,35	30	3	0,5	14
15-0239-M-019	19	19A	5	1	80	3	0,5	14
15-0239-M-020	20	20A	19	6,35	80	3	0,5	14
15-0239-M-021	21	21A	6	1	30	4	0,5	14
15-0239-M-022	80	22A	17	6,35	30	4	0,5	14
15-0239-M-023	23	23A	20	1	80	4	0,5	14
15-0239-M-024	24	24A	33	6,35	80	4	0,5	14
15-0239-M-025	25	25A	23	1	30	3	1	14
15-0239-M-026	26	26A	22	6,35	30	3	1	14
15-0239-M-027	27	27A	15	1	80	3	1	14
15-0239-M-028	28	28A	21	6,35	80	3	1	14
15-0239-M-029	29	29A	13	1	30	4	1	14
15-0239-M-030	30	30A	18	6,35	30	4	1	14
15-0239-M-031	31	31A	7	1	80	4	1	14
15-0239-M-032	32	32A	3	6,35	80	4	1	14
15-0239-M-033	33	33A	35	3,2	55	3,5	0,75	12
15-0239-M-034	34	34A	11	3,2	55	3,5	0,75	12
15-0239-M-035	35	35A	37	3,2	55	3,5	0,75	12
15-0239-M-036	36	36A	27	3,2	55	3,5	0,75	12
15-0239-M-037	37	37A	2	3,2	55	3,5	0,75	12

Table 2A. Extra samples cut with increased cutting speed. Not included in the original test set-up and not evaluated in the result part in the report.

Mount no	Exp No	Exp Name	Run Order	Material thickness	Lens focal lenght	Beam power	Cutting speed	Gas pressure
15-0239-M-038	38	38A		1	30	3	0,5	14
15-0239-M-039	39	39A		1	30	3	0,5	14
15-0239-M-040	40	40A		3,2	55	3,5	0,75	16
15-0239-M-041	41	41A		1	55	3,5	1,5	12
15-0239-M-042	42	42A		1	55	3,5	2	12
15-0239-M-043	43	43A		1	55	3,5	2,5	12
15-0239-M-044	44	44A		3,2	55	3,5	1,5	12
15-0239-M-045	45	45A		3,2	55	3,5	2	12
15-0239-M-046	46	46A		3,2	55	3,5	2,5	12
15-0239-M-047	47	47A		6,35	55	3,5	1,5	12
15-0239-M-048	48	48A		6,35	55	3,5	2	12
15-0239-M-049	49	49A		6,35	55	3,5	2,5	12
15-0239-M-050	50	50A		6,35	55	3,5	3	12

A3. Experimental set-up for the samples cut with Nitrogen as assist gas.

Table 3A. Test plan showing the different parameter levels used

Mount no	Exp No	Exp Name	Run Order	Materil thickness	Lens focal length	Beam power	Cutting speed	Gas pressure
15-0239-M-051	1	1N	1	1	30	3	0,5	14
15-0239-M-052	2	2N	14	6,35	30	3	0,5	14
15-0239-M-053	3	3N	27	1	80	3	0,5	14
15-0239-M-054	4	4N	20	6,35	80	3	0,5	14
15-0239-M-055	5	5N	28	1	30	4	0,5	14
15-0239-M-056	6	6N	10	6,35	30	4	0,5	14
15-0239-M-057	7	7N	34	1	80	4	0,5	14
15-0239-M-058	8	8N	8	6,35	80	4	0,5	14
15-0239-M-059	9	9N	24	1	30	3	1	14
15-0239-M-060	10	10N	7	6,35	30	3	1	14
15-0239-M-061	11	11N	15	1	80	3	1	14
15-0239-M-062	12	12N	21	6,35	80	3	1	14
15-0239-M-063	13	13N	30	1	30	4	1	14
15-0239-M-064	14	14N	26	6,35	30	4	1	14
15-0239-M-065	15	15N	18	1	80	4	1	14
15-0239-M-066	16	16N	31	6,35	80	4	1	14
15-0239-M-067	17	17N	32	1	30	3	0,5	18
15-0239-M-068	18	18N	35	6,35	30	3	0,5	18
15-0239-M-069	19	19N	23	1	80	3	0,5	18
15-0239-M-070	20	20N	33	6,35	80	3	0,5	18
15-0239-M-071	21	21N	4	1	30	4	0,5	18
15-0239-M-072	22	22N	37	6,35	30	4	0,5	18
15-0239-M-073	23	23N	19	1	80	4	0,5	18
15-0239-M-074	24	24N	11	6,35	80	4	0,5	18
15-0239-M-075	25	25N	22	1	30	3	1	18
15-0239-M-076	26	26N	13	6,35	30	3	1	18
15-0239-M-077	27	27N	17	1	80	3	1	18
15-0239-M-078	28	28N	25	6,35	80	3	1	18
15-0239-M-079	29	29N	6	1	30	4	1	18
15-0239-M-080	30	30N	12	6,35	30	4	1	18
15-0239-M-081	31	31N	29	1	80	4	1	18
15-0239-M-082	32	32N	3	6,35	80	4	1	18
15-0239-M-083	33	33N	9	3,2	55	3,5	0,75	16
15-0239-M-084	34	34N	16	3,2	55	3,5	0,75	16
15-0239-M-085	35	35N	36	3,2	55	3,5	0,75	16
15-0239-M-086	36	36N	5	3,2	55	3,5	0,75	16
15-0239-M-087	37	37N	2	3,2	55	3,5	0,75	16

Table 4A. Extra samples cut with increased cutting speed. Not included in the original test set-up and not evaluated in the result part in the report

Mount no	Exp No	Exp Name	Material thickness	Lens focal lenght	Beam power	Cutting speed	Gas pressure
15-0239-M-088	38N	38N	1	30	3	0,5	16
15-0239-M-089	39N	39N	3,2	55	3,5	1	18
15-0239-M-090	40N	40N	1	55	3,5	1,5	16
15-0239-M-091	41N	41N	1	55	3,5	2	16
15-0239-M-092	42N	42N	1	55	3,5	2,5	16
15-0239-M-093	43N	43N	3.2	55	3,5	1,5	16
15-0239-M-094	44N	44N	3,2	55	3,5	2	16
15-0239-M-095	45N	45N	3.2	55	3,5	2,5	16
15-0239-M-096	46N	46N	6,35	80	3	1	14
15-0239-M-097	47N	47N	6,35	80	3	1	18

8.2 Appendix B: Sample preparation protocol

Table 1B. Instructions for grinding, polishing and etching.

Sample preparation							
Grinding							Polishing
Step	1	2	3	4	5	6	7
Abrasive	80	120	240	800	2500	4000	OPS (colloidal silica)
Lubricant	water	water	water	water	water	water	
RPM	300	300	300	300	300	300	150
Time (s)	60	60	60	60	30	30	300
Force (N/ea)	35	35	35	35	35	35	35
Etching							
Etchant	Kroll's 192						
Time (s)	20						

8.3 Appendix C: Location of HAZ measurements

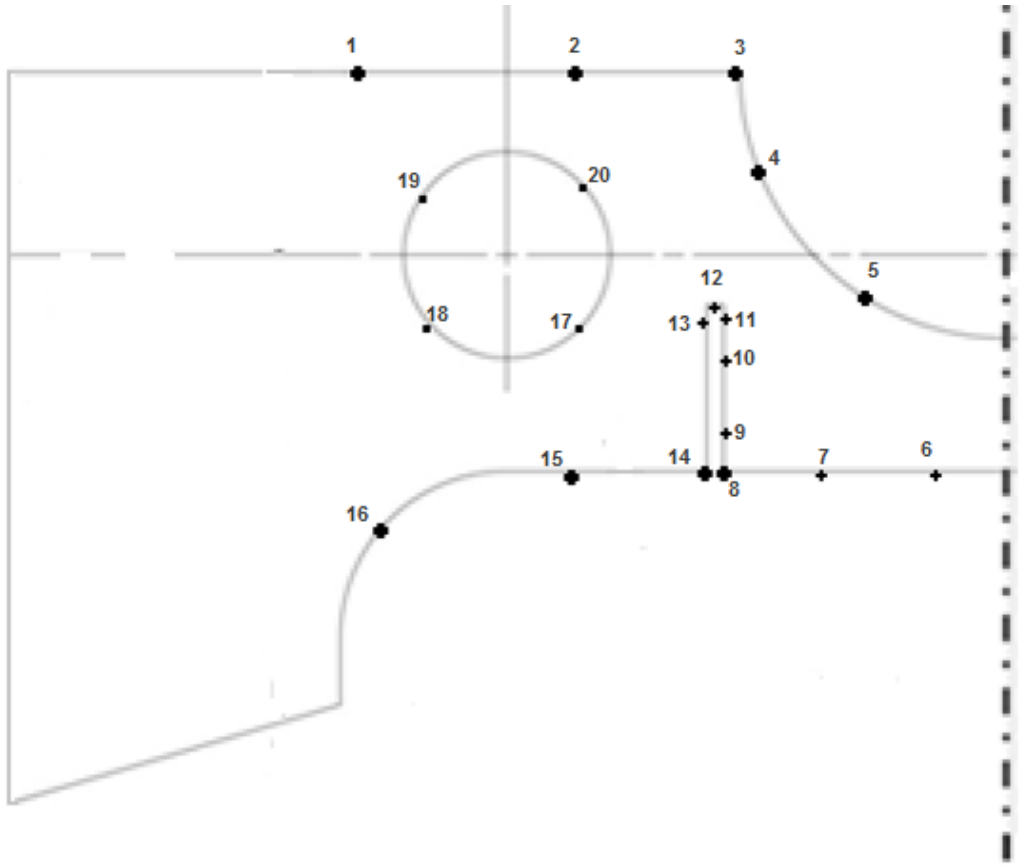

Figure 1C. Locations on the sample from which the HAZ was measured.

8.4 Appendix D: Locations for surface irregularity measurements

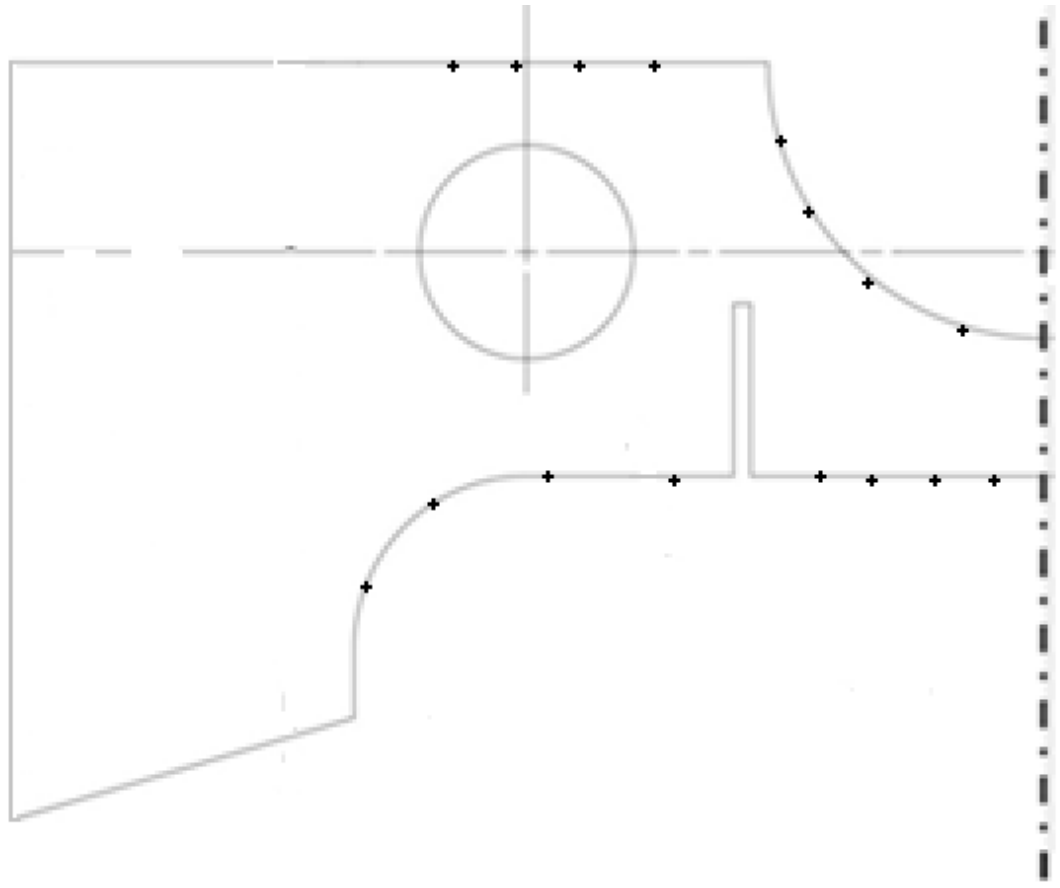

Figure 1D. Locations on the sample where surface irregularity measurements were taken.